PHOTOTHERMAL, ELECTROCHEMICAL AND ANTIBACTERIAL POTENTIAL OF ZINC FERRITE/SILVER/SILVER CHLORIDE NANOCOMPOSITE

PROJECT REPORT

Submitted by

FATHIMA NOOFA UKO

Register No. : AM23PHY006

Under guidance of

Dr. MINU PIUS

Assistant Professor

Department of Physics
St. Teresa's College (Autonomous), Ernakulam

Kochi – 682011

Submitted to
Mahatma Gandhi University, Kottayam

In partial fulfillment of the requirements for the award of the degree of

MASTER OF SCIENCE IN PHYSICS

DEPARTMENT OF PHYSICS

ST. TERESA'S COLLEGE (AUTONOMOUS), ERNAKULAM

PHOTOTHERMAL, ELECTROCHEMICAL AND ANTIBACTERIAL POTENTIAL OF ZINC FERRITE/SILVER/SILVER CHLORIDE NANOCOMPOSITE

PROJECT REPORT

Submitted by

FATHIMA NOOFA UKO

Register No. : AM23PHY006

Under guidance of

Dr. MINU PIUS

Assistant Professor

Department of Physics
St. Teresa's College (Autonomous), Ernakulam

Kochi – 682011

Submitted to
Mahatma Gandhi University, Kottayam

In partial fulfillment of the requirements for the award of the degree of

MASTER OF SCIENCE IN PHYSICS

DEPARTMENT OF PHYSICS

ST. TERESA'S COLLEGE (AUTONOMOUS), ERNAKULAM

DEPARTMENT OF PHYSICS
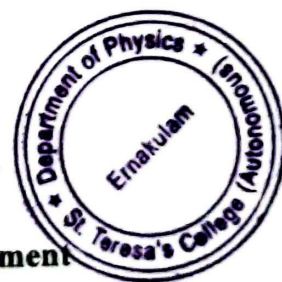
ST. TERESA'S COLLEGE (AUTONOMOUS), ERNAKULAM

CERTIFICATE

This is to certify that the project report entitled "PHOTOTHERMAL, ELECTROCHEMICAL AND ANTIBACTERIAL POTENTIAL OF ZINC FERRITE/SILVER/SILVER CHLORIDE NANOCOMPOSITE" is an authentic work done by FATHIMA NOOFA UKO (AM23PHY006) under my guidance at Department of Physics, St. Teresa's College (Autonomous), Ernakulam for the partial fulfillment of the requirements for the award of the Degree of Master of Science in Physics during the year 2024-25. The work presented in this dissertation has not been submitted for any other degree in this or any other university.

Supervising Guide

Dr. MINU PIUS

Head of the Department

DR. MARY VINAYA

Place: Ernakulam

Date: 02 - 05 - 2025

2

DEPARTMENT OF PHYSICS
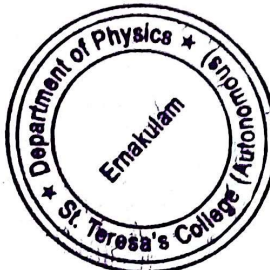
ST. TERESA'S COLLEGE (AUTONOMOUS), ERNAKULAM

M.Sc. PHYSICS

PROJECT REPORT

Name : FATHIMA NOOFA UKO

Register No. : AM23PHY006

Year of Work : 2024-2025

This is to certify that the project entitled "PHOTOTHERMAL, ELECTROCHEMICAL AND ANTIBACTERIAL POTENTIAL OF ZINC FERRITE/SILVER/SILVER CHLORIDE NANOCOMPOSITE" is an authentic work done by FATHIMA NOOFA UKO.

Staff member in-charge

Dr. MINU PIUS

Assistant Professor

Head of the Department

Dr. MARY VINAYA

Assistant professor

Submitted for the university examination held at St. Teresa's College (Autonomous), Ernakulam.

DATE: 02-05-2025

EXAMINERS :

3

DECLARATION

I, FATHIMA NOOFA UKO, final year student of Department of Physics and Centre for Research, St.Teresa's College (Autonomous), Ernakulam, hereby declare that the project report entitled **"PHOTOTHERMAL, ELECTROCHEMICAL AND ANTIBACTERIAL POTENTIAL OF ZINC FERRITE/SILVER/SILVER CHLORIDE NANOCOMPOSITE"** is a bonafide work done by me under the guidance and supervision of **Dr. MINU PIUS,** Assistant professor, Department of Physics, St. Teresa's College (Autonomous), Ernakulam in partial fulfilment of the requirement for the award of degree of M.Sc. PHYSICS. I further declare that this work is not submitted for any other degree or certification elsewhere.

PLACE : ERNAKULAM

DATE : 02 - 05 - 2025

FATHIMA NOOFA UKO

AM23PHY006

ACKNOWLEDGEMENT

I would like to express my sincere gratitude to Dr. MINU PIUS, Assistant Professor, Department of Physics and Centre for Research, St. Teresa's College (Autonomous), Ernakulam for her valuable guidance, continuous support, and insightful suggestions throughout the course of this project. Her mentorship has been instrumental in shaping both the direction and quality of this research work.

I would also like to extend my gratitude to Dr. MARY VINAYA , Head of the Department of Physics and Centre for Research, St. Teresa's College (Autonomous), Ernakulam, for providing the necessary facilities and for fostering a supportive academic environment.

I am grateful to all the teaching and non teaching staffs of the department for their assistance and cooperation during various stages of the project. I also extend my heartfelt gratitude to my friends for their encouragement, shared knowledge, and helpful discussions, which greatly enriched this experience.

Finally, I am deeply grateful to my parents for their unwavering support, understanding, and motivation throughout this academic journey.

ST.TERESA'S COLLEGE (AUTONOMOUS) ERNAKULAM

Certificate of Plagiarism Check for Dissertation

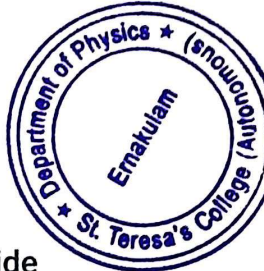|	
Author Name	FATHIMA NOOFA UKO , SNIYA V S.
Course of Study	M.Sc. Physics
Name of Guide	Dr. Minu Pius
Department	Department of Physics & Centre for Research
Acceptable Maximum Limit	20
Submitted By	library@teresas.ac.in
Paper Title	SYNTHESIS AND CHARACTERIZATION OF ZINC FERRITE/SILVER/SILVER CHLORIDE NANOCOMPOSITES AT DIFFERENT CALCINATION TEMPERATURES
Similarity	4% AI-19%
Paper ID	3558594
Total Pages	44
Submission Date	2025-04-29 14:54:32

Signature of Student

Signature of Guide

Checked By
College Librarian

PHOTOTHERMAL, ELECTROCHEMICAL AND ANTIBACTERIAL POTENTIAL OF ZINC FERRITE/SILVER/SILVER CHLORIDE NANOCOMPOSITE

ABSTRACT

In this study, we report the synthesis of a zinc ferrite/silver/silver chloride nanocomposite at various calcination temperatures using co-precipitation method. The phase purity and crystallinity of the nanocomposites were confirmed through X-ray diffraction (XRD) analysis. Optical properties were investigated using Fourier Transform Infrared Spectroscopy (FTIR) to identify functional groups and Ultraviolet-Visible (UV-Vis) absorption spectroscopy to determine the bandgap of the materials. Magnetic characterization, conducted with a Vibrating Sample Magnetometer (VSM), revealed the superparamagnetic behavior of the samples. The results demonstrate the successful synthesis of the nanocomposites with tunable optical and magnetic properties, which could be promising for various applications in catalysis, sensors and environmental remediation.

Contents

CHAPTER 3

RESULTS AND DISCUSSION

CHAPTER 1

INTRODUCTION

Nanoparticle-metal oxides are an increasingly important category of the materials in healthcare and research applications. Ferrite nanoparticles have been studied recently and also developed more and more. In terms of catalytic properties, ferrite nanoparticles are frequently being studied, especially in environmental applications like pollutant breakdown.

Quite meaningful in several magnetic materials, sensors, catalysts, and electrocatalytic devices, zinc ferrite has become useful throughout a range of applications. This is caused by extraordinary mechanical stability and extraordinary thermal stability, as well as high energy transfer efficiency, in addition to its distinctive ability for the control of magneto-optical properties. Photocatalytic activity is exhibited by certain Silver nanoparticles and antimicrobial properties are possessed by various Silver Chloride nanoparticles. $ZnFe_2O_4/Ag/AgCl$ nanocomposites have semiconductor-metal ($ZnFe_2O_4/Ag$) junctions, as well as Schottky (Ag/AgCl). These junctions serve to improve the process of charge transfer and substantially increase the electrocatalytic performance within the nanocomposites specifically for OER.
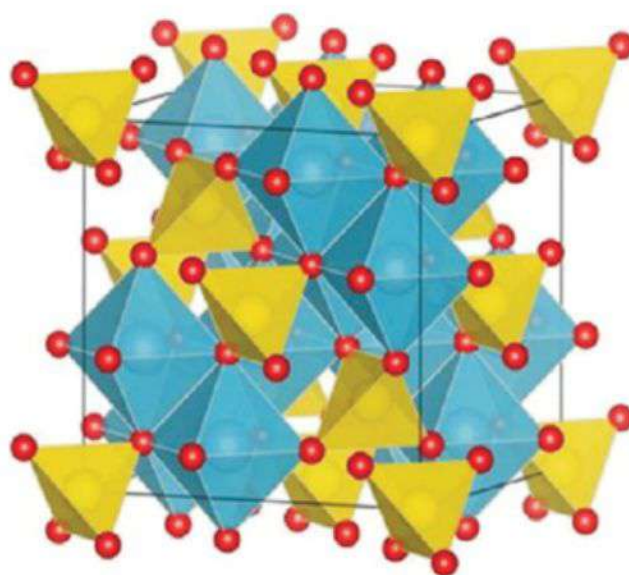
1.1. ZINC FERRITE

[1]

Fig.1 Structure of Zinc Ferrite

---

[1] https://www.intechopen.com/media/chapter/58926/media/F1.png

Zinc Ferrite nanoparticles ($ZnFe_2O_4$) have a cubic spinel crystal structure, where zinc and irons are distributed in such a way that it enhances the magnetic behavior. Formula of zinc ferrite is AB_2O_4; in which A denotes a divalent metal ion (Zn^{2+}), B denotes a trivalent metal ion (Fe^{3+}), and O is the oxygen ion. These zinc ferrite nanoparticles have face-centered cubic (FCC) structure.

There are two kinds of spinal structures:

Normal spinal in which A^{2+} ions reside in tetrahedral sites and B^{3+} ions reside in octahedral sites.

Inverse spinel in which half of the B^{3+} ions reside in tetrahedral sites, and the rest along with A^{2+} ions reside in octahedral sites.
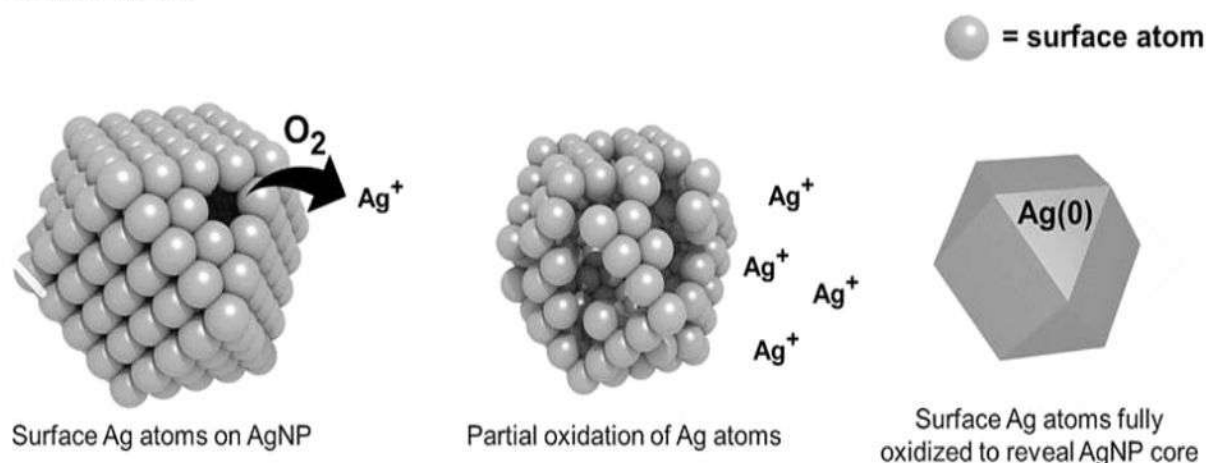
Zinc Ferrite has a normal spinel structure in which Zn^{2+} ions reside in tetrahedral sites and Fe^{3+} ions reside in octahedral sites. The oxygen creates a closely packed lattice. 1/8 of tetrahedral sites are occupied by Zn^{2+} and 1/2 of octahedral sites are occupied by Fe^{3+}. When Zinc Ferrite are nanoparticles the surface-to-volume ratio increases which affects their magnetic and optical properties, structural defects, surface strain, and cation redistribution. This affects their magnetic and electronic behaviour, and catalytic activity.

Bulk $ZnFe_2O_4$ is antiferromagnetic or weakly magnetic in nature, but nanoparticles can show superparamagnetic behaviour. Superparamagnetism or improved ferrimagnetism is shown at room temperature upon synthesis within nanoparticle form. Biomedical applications do find this superparamagnetic nature quite helpful for them. ZnFe2O4 does have a semiconducting band gap ($\sim$ 1.9 – 2.2 eV), and so it is useful in optoelectronic and photocatalysis applications. Being biocompatible as well as chemically stable, it is quite suitable for biomedical and environmental applications.

$ZnFe^2O_4$ exhibits superb thermal stability as well as corrosion resistance, so they are powerful under extreme environmental conditions. On account of these attributes, they may be used catalytically when elevated temperature functioning matters. They do have outstanding biocompatibility, low toxicity, as well as controllable magnetic properties, also high chemical stability, and high electrical resistivity in comparison to other ferrites. Also, they do have a lower curie temperature in comparison with the other transition metals ferrites.

$ZnFe_2O_4$ exhibits very unique structural and magnetic and electronic properties in regard to a wide range of the applications. They have an average bandgap and thus they are active under visible light for the photocatalytic applications. Hydrogen production as well as the breakdown of dyes, pesticides, as well as pharmaceutical contaminants specifically in water all come from their particular use for dehydration of various organic pollutants. Wastewater treatment and dye degradation, organic synthesis reactions, and oxidation and reduction reactions are examples among chemical reactions, where they act as an efficient heterogeneous catalyst. Because of their high surface area, they increase catalytic performance and still remain stable upon reactions.Recent studies suggest zinc ferrites exhibit antimicrobial activity against a range of bacteria and fungi, making them useful in coatings, packaging, and medical device applications.

1.2. SILVER

= surface atom

Surface Ag atoms on AgNP

Partial oxidation of Ag atoms

Surface Ag atoms fully oxidized to reveal AgNP core

[2]

Fig.2 Structure of Silver

Sliver (Ag) is face-centred cubic (FCC) crystal structure. Each Ag atom is surrounded by 12 nearest neighbours which gives a highly symmetrical dense structure thus contributing to the material's high mechanical strength and conductivity. Nanoscale silver provides unique optical, electronic, and catalytic properties not observed in bulk. Silver has high electrical and thermal conductivity of all metals. They exhibit unique optical properties due to surface plasmon resonance (SPR) which refers to the collective oscillation of conduction electrons at nanoparticle surface when excited by light at specific wavelengths that results in intense absorption and scattering in the visible region giving silver nanoparticle their characteristic yellow to brown color in colloidal solutions. Silver nanoparticles are mostly thermal and electrical conductive metal which is critical in applications like transparent electrodes, flexible electronics, and nanoscale circuits. One of silver's most important properties is its antimicrobial activity. This property is made use in a wide range of medical and consumer products, water purification systems, and antimicrobial fabrics, etc. Silver nanoparticles possess a high surface energy and a large number of active sites, enabling them to act as effective catalysts in many chemical reactions including oxidation and reduction reactions.

Silver particularly in the form nanoparticles shows enhanced photocatalytic activity when combined with semiconductors such as ZnO or $ZnFe_2O_4$. Even though silver itself is not a traditional semiconductor photocatalyst, it serves as co-catalyst or photosensitizer that boosts the overall photocatalytic efficiency through several mechanisms such as; Surface Plasmon Resonance (SPR), electron trap and charge separation and generation of reactive oxygen species (ROS). Due to these properties silver has many applications like in water purification, air purification, self-cleaning surfaces, and antibacterial surfaces

---

[2]
https://sustainabilitycommunity.springernature.com/cdn-cgi/image/metadata=copyright,fit=scale-down,format=auto,sharpen=1,quality=95/https://images.zapnito.com/uploads/67hKmtIIQ06XwFLKB8nT_image_1%20(2).jpg

1.3. SILVER CHLORIDE
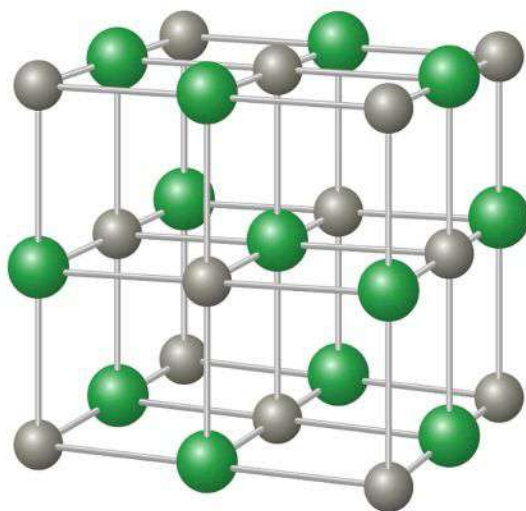
Fig.3 Structure of Silver Chloride

Silver Chloride (AgCl) is a face centred cubic (FCC) inorganic compound similar to sodium chloride (NaCl) structure. Each silver ion (Ag^+) is surrounded by six chloride ions (Cl^-) forming a tightly packed highly symmetrical crystal lattice. At nanoscale, these particles exhibit high surface-to-volume ratio, which increases its reactivity and ion release. Their nano size can lead to slight lattice distortions and more active surface sites, which improves their interaction with biological systems. It is less soluble in water but dissolves in ammonia, cyanide, or concentrated chloride solutions. Its poor solubility contributes to its slow release of silver ions - a key feature in its antimicrobial property. It is highly sensitive towards light as it decomposes in light into metallic silver and chloride gas, which is the basis for its historical use in photographic films. They partially reduce metallic silver under light, creating Ag/AgCl hybrid structures which enhance antimicrobial and photocatalytic properties. Silver nanoparticles show strong broad spectrum antimicrobial activity against bacteria, fungi, and some viruses due to disruption of membranes of microbes, generation of reactive oxygen species (ROS) and interactions with protein and DNA. It shows ionic conductivity in solid form at elevated temperatures, useful in electrochemical applications.

1.4. ZINC FERRITE/SILVER/SILVER CHLORIDE NANOCOMPOSITES

The combination of zinc ferrite ($ZnFe_2O_4$), silver (Ag), silver chloride (AgCl) into a nanocomposite results in a multifunctional material with significantly enhanced properties. Each component contributes individually to the nanocomposite's overall behaviour, and their

---

[3]

interaction leads to symbiotic effects that improve photocatalytic, antimicrobial, magnetic, and electronic performance.

Zinc ferrite/silver/silver chloride nanocomposites have been used instead of individual components due to synergistic effects between materials enhance their performance in specific applications such as photocatalysis, antimicrobial activity, and sensing.When they are used together; their photocatalytic activity is enhanced, their antimicrobial properties will improve and and also there will be magnetic recoverability.

Zinc ferrite/silver/silver chloride nanocomposites consist of $ZnFe_2O_4$ nanoparticles as a core, with Ag and AgCl nanoparticles arranged on the surface. Their large surface area as well as nano size create many active sites so effective photocatalytic and antibacterial reactions are enabled. Because Ag and AgC nanoparticles are distributed in an even way on $ZnFe_2O_4$, agglomeration is prevented, and also the functionalities of each component are preserved as well.

Band gap of the ZnFe2O4 is suited for absorption of visible light. Surface plasmon resonance (SPR) is greatly exhibited by Ag nanoparticles, which in turn improves light harvesting and also creates localized electromagnetic fields that greatly increase the efficiency of photocatalytic activity. Ag acts in a combination as a conduction band between $ZnFe_2O_4$ and AgCl, and it eases the fast electron transfer and suppresses the photogenerated electron-hole pairs recombination, which the single component photocatalysis commonly limits. Electrons originating from AgCl's conduction band recombine with valence band holes of $ZnFe_2O_4$ by means of AgCl nanoparticles acting as mediators in which the nanocomposite operates through Z-scheme photocatalytic mechanism, in which $ZnFe_2O_4$ absorbs visible light so it can generate electron-hole pairs, and in which AgCl absorbs light as well as produces charge carriers. This preserves strong oxidative as well as reduction potentials, thus improving the production of several reactive oxygen species (ROS) for degeneration. This also improves with the production of pollutants and microbial inactivation. $ZnFe_2O_4$ at the nanoscale acts as a soft magnet, showing superparamagnetic traits. The photocatalyst separates effortlessly from within treated solutions because of this magnetic property with an external magnetic field making the system eco-friendly and reusable.

AgCl slowly and also controllably releases Ag+ ions in this process. This action ensures durable antimicrobial effects, and neither does it cause toxic surrounding environments. Nanocomposite generates an amount of ROS under the presence of visible light, and this leads to their destruction.

AgCl is fairly stable under the dark conditions but might convert to metallic Ag under a light partially improving performance while $ZnFe_2O_4$is thermally stable and chemically resistant. The nanocomposite retains durability and function over time, permitting frequent use maintaining its effectiveness.

There are several synthesis methods for synthesis of Zinc ferrite/silver/silver chloride nanocomposites such as; Hydrothermal method, sol gel method, electrochemical deposition, co precipitation method,etc. Among these we use co precipitation method due to their simplicity and low cost, mild reaction condition, homogeneous mixing at atomic level, particle size control, high purity, etc.

1.5. OBJECTIVE

The increasing demand for multifunctional nanomaterials with enhanced photocatalytic, magnetic, and antimicrobial properties has driven broad research into hybrid nanocomposites. Zinc ferrite/silver/silver chloride nanocomposites have emerged as top prospects due to their synergistic behaviour, combining the semiconducting and magnetic nature of zinc ferrite with plasmonic and antimicrobial capabilities of silver and silver chloride.

This thesis focuses on the synthesis and characterization of zinc ferrite/silver/silver chloride nanocomposites using the co-precipitation method, which is a simple, cost effective and scalable technique that allows for uniform distribution of nanoparticles and controlled stoichiometry. The co-precipitation method enables the parallel formation of zinc ferrite and on site incorporation of silver and silver chloride, facilitating strong interfacial contact and improved functional performance.

The nanocomposites were subjected to detailed physicochemical characterization using techniques such as; X-ray diffraction (XRD), Fourier-transform infrared spectroscopy (FTIR), UV-Vis spectroscopy, Vibrating sample magnetometer (VSM) and photocatalytic and antibacterial tests to evaluate functional performance.

1.6. LITERATURE REVIEW

Zinc ferrite nanoparticles exhibited favourable biomedical properties, showing dose-dependent cytotoxicity towards human dermal fibroblasts in prestoblue and live/dead assays. Hemocompatibility tests showed that nanoparticles did not cause significant red blood cell break up to 1000 µg/mL. Antibacterial showed strong, dose-dependent antimicrobial action against Gram-positive and Gram-negative bacteria, primordially through mechanisms like membrane damage, protein leakage, and reactive oxygen species (ROS) generation, with greater performance against Gram-positive strains. Besides, an in vitro scratch assay showed that zinc ferrite nanoparticles enhanced cell migration and proliferation, promoting artificial wound closure. Hence zinc ferrite nanoparticles have potential to be used as a future antimicrobial and wound healing drug [1]. Zinc ferrite coated with natural CT polymer performs an excellent antibacterial agent against both Gram-positive and Gram-negative bacteria. CT-$ZnFe_2O_4$ nanoparticles prevent the biofilm formation more than 65% and reduce recognised biofilm up to 50% at a respective minimum inhibitory concentration (MIC). This suggests an exciting opportunity in antimicrobial therapy like antibacterial coatings that wound care and target drug delivery in biofilm treatment [2].

The antibacterial control tests on triangular and spherical silver nanoparticles of different sizes revealed that they were toxic to both P.aeruginosa and E.coli and their antibacterial efficiency was found to be size and shape dependent. The smaller sized spherical silver nanoparticles showed higher antiseptic efficiency than that of the triangular ones, while larger spherical silver nanoparticles showed efficient antibacterial action than triangle shaped silver nanoparticles against both bacterial strains. Silver nanoparticles with efficient shape and size could be possible options for antibiotics which have encountered more bacterial resistance [3]. The dynamics of decomposition are firmly dependent on Cl/Ag ratio and can be analyzed using the thermodynamically expected speciation of silver in the presence of chloride. The toxicity of silver nanoparticles to E.coli at various Cl^- concentrations is controlled by the amount of dissolved $AgCl_x^{(x-1)-}$ species advising an ion effect rather than a nanoparticle effect [4].Surface level reactions of silver nanoparticles are an important element to explain their behavior, fate and action, and thereby their antibacterial activity. Phenomena that can occur that lead to their aggregation are an oxidation dissolution, formation of a passivating layer, puncturation of this layer by other chemical species, redeposition of silver and formation of bridging material between particles [5].Various methods are used to evaluate nanoparticle size and surface properties and there is a lack of understanding of the character of proteins that wrap the nanoparticles. In addition, variations in antimicrobial assays, bacterial strains, and protocols used in studies make it difficult to compare results across research. The complete nanoparticle characterization and standardized microbiological methods are necessary for obtaining consistent antimicrobial data on biogenic silver based nanoparticles [6].

Zinc ferrite ($ZnFe_2O_4$) thin films were deposited on indium tin oxide and quartz substrates by RF sputtering at room temperature under different argon/oxygen gas ratios: 1:0 (Z–Ar), 1:1 (Z–Ar:O), and 0:1 (Z–O). Grazing incidence X-ray diffraction (GIXRD) at a 0.400° angle confirmed their polycrystalline structure. X-ray photoelectron spectroscopy (XPS) analysis of Zn 2p, Fe 2p, and O 1s regions showed that the Z–Ar film had more lattice oxygen vacancies compared to the Z–O film.The presence of vacancies in the Z–Ar film reduced the bandgap to 2.05 eV, while the Z–O film showed a bandgap of 2.36 eV. Electrochemical testing revealed that the Z–Ar film achieved a ~12.5% lower overpotential at $10\,mA\,cm^{-2}$, an eightfold higher current density at 520 mV overpotential, and a 71.9% increase in donor density, compared to the Z–O film.These results suggest that the Z–Ar film follows a lattice oxygen participation mechanism during the oxygen evolution reaction (OER), whereas the Z–O film operates through the conventional adsorbate evolution mechanism. The study highlights how tuning the gas atmosphere during deposition can significantly impact the structural, optical, and electrochemical properties of zinc ferrite thin films [7].

Water splitting is a key technology for storing renewable energy sources like solar and wind in the form of hydrogen fuel. However, the oxygen evolution reaction (OER) remains a major challenge due to its slow kinetics. Although metal oxides were identified as OER

catalysts decades ago, recent interest in sustainable energy has revived research in this area. This study highlights important developments, including a better theoretical understanding of OER mechanisms, the discovery of activity trends among different oxides, and advancements in in situ and operando characterization methods. These tools have served well enough to clarify the very true nature of active catalytic sites. Additionally, these researchers do explore several new oxide materials, and this opens up new opportunities for those researchers to design catalysts that could be more efficient and also more stable. The literature stresses that which a number of researchers have achieved, and also those difficulties that do remain; particularly researchers do have a need for long-term stability as well as deeper mechanistic understandings in order that certain applications are able to be practical at a large scale [8].

The oxygen evolution reaction (OER) is a certain key step for several renewable energy systems, such as water splitting, metal-air batteries, and fuel cells. For very large-scale applications, quite efficient in addition to cost-effective, stable electrocatalysts should be developed. Interest regarding the utilization of non-noble metals for OER catalysis has been measurably growing recently via promising activity besides abundance. In this review, a discussion of the recent progress that has been made in non-noble metal-based catalysts is included, with a focus upon the nanostructured materials, such as cobalt, nickel, manganese, iron, copper, and zinc oxides, along with complex structures such as spinels, perovskites, and layered double hydroxides. It does stress all of the important elements affecting catalyst behavior. Nanostructure design, and the control of crystal phase and of morphology, creation of defects, as well as doping strategies, are but a few of the factors. Also, techniques such as engineering of strain inside of the materials and also forming of mixed-metal systems are fully explored here. Understandings into a number of future research directions so as to develop improved catalysts for practical energy storage applications [9], as well as important challenges still faced, like that of improving long-term stability with efficiency, are finally outlined in the review.

The oxygen evolution reaction (OER) plays a key role in pushing forward sustainable energy tech such as metal–air batteries and water splitting. A major hurdle still remains, even though some meaningful strides have been made in developing OER catalysts; long-term stability as well as high catalytic activity must be fully balanced. Often, the improvement of one comes at the cost of the other as a trade-off still limiting real-world applications. Within this Perspective, we highlight several key findings from both experimental research and theoretical studies as we dive into the complex relationship between activity and stability. We especially observe performance of electrodes under differing electrochemical states. This is especially true in the instance that the environments are acidic and alkaline. We propose now a more unified comprehension of all the mechanisms which are driving this activity–stability tension by weaving together all of the latest advancements within catalyst design. Finally, we outline a number of strategies that may rationally develop the next-generation OER catalysts — catalysts that deliver both a high level of performance and a lasting level of durability [10].

1.7. REFERENCE

[1] Haghniaz, R., Rabbani, A., Vajhadin, F., Khan, T., Kousar, R., Khan, A. R., ... & Wahid, F. (2021). Anti‑bacterial and wound healing‑promoting effects of zinc ferrite nanoparticles. *Journal of nanobiotechnology*, *19*, 1-15.

[2] Sharma, R. P., Raut, S. D., Kadam, A. S., Mulani, R. M., & Mane, R. S. (2020). In-vitro antibacterial and anti-biofilm efficiencies of chitosan-encapsulated zinc ferrite nanoparticles. *Applied Physics A*, *126*, 1-9.

[3] Raza, M. A., Kanwal, Z., Rauf, A., Sabri, A. N., Riaz, S., & Naseem, S. (2016). Size-and shape-dependent antibacterial studies of silver nanoparticles synthesized by wet chemical routes. *Nanomaterials*, *6*(4), 74.

[4] Levard, C., Mitra, S., Yang, T., Jew, A. D., Badireddy, A. R., Lowry, G. V., & Brown Jr, G. E. (2013). Effect of chloride on the dissolution rate of silver nanoparticles and toxicity to E. coli. *Environmental science & technology*, *47*(11), 5738-5745.

[5] Le Ouay, B., & Stellacci, F. (2015). Antibacterial activity of silver nanoparticles: A surface science insight. *Nano today*, *10*(3), 339-354.

[6] Durán, N., Nakazato, G., & Seabra, A. B. (2016). Antimicrobial activity of biogenic silver nanoparticles, and silver chloride nanoparticles: an overview and comments. *Applied microbiology and biotechnology*, *100*, 6555-6570.

[7] Singh, A. K., Kumar, S., Yadav, B. S., Vishwakarma, A. K., & Kumar, N. (2023). Evidence of oxygen evolution over sputtered zinc ferrite (ZnFe2O4) thin film by enhanced lattice oxygen participation. *Applied Physics Letters*, *123*(3).

[8] Song, F., Bai, L., Moysiadou, A., Lee, S., Hu, C., Liardet, L., & Hu, X. (2018). Transition metal oxides as electrocatalysts for the oxygen evolution reaction in alkaline solutions: an application-inspired renaissance. *Journal of the American Chemical Society*, *140*(25), 7748-7759.

[9] Vazhayil, A., Vazhayal, L., Thomas, J., & Thomas, N. (2021). A comprehensive review on the recent developments in transition metal-based electrocatalysts for oxygen evolution reaction. *Applied surface science advances*, *6*, 100184.

[10] Park, W., & Chung, D. Y. (2024). Activity–Stability Relationships in Oxygen Evolution Reaction. *ACS Materials Au*, *5*(1), 1-10.

CHAPTER 2

EXPERIMENTAL DETAILS

2.1 SYNTHESIS

Synthesis of Zinc ferrite/Silver/Silver chloride

Solution mixing → Precipitation → Digestion at 100°C →
(magnetic stirring at 80°C)

Sample ⇐ Calcination and grinding ⇐ Drying at 100°C ⇐ Centrifuging (at 6000 rpm)
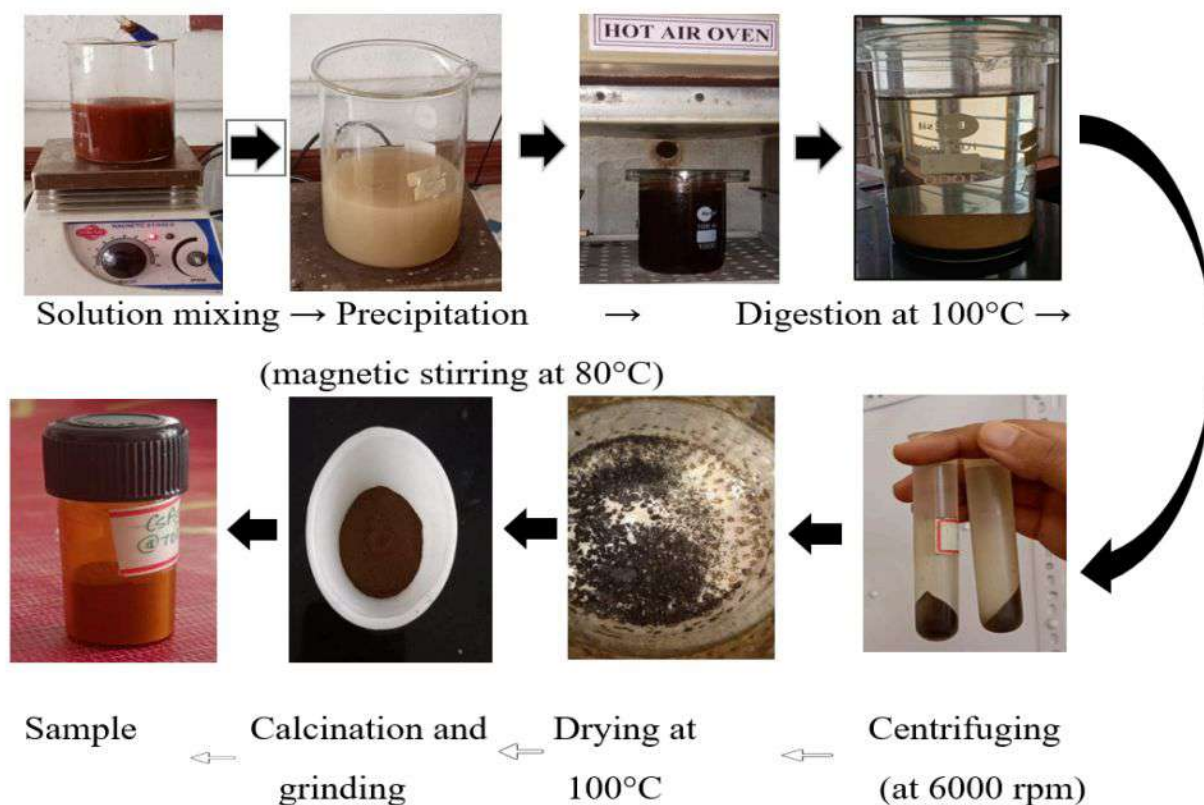
Chemical reactions with molar ratios that used for the synthesis of Zinc ferrite/silver/silver chloride nanocomposite:

$$2 \, FeCl_3 . 6H_2O + ZnCl_2 + 8 \, NaOH \rightarrow ZnFe_2O_4 + 8NaCl + 10H_2O \qquad 2.1$$

$$FeCl_3 . 6H_2O : ZnCl_3 : NaOH = 0.1M : 0.05M : 0.4M \qquad 2.2$$

$$AgNO_3 : TSC = 0.01M : 0.1M \qquad 2.3$$
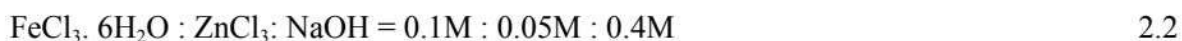
2.1.1 CO-PRECIPITATION METHOD

The co-precipitation method is a widely used chemical synthesis technique for preparing metal oxide nanoparticles. In this method, metal salts are dissolved in an aqueous solution and a precipitating agent, such as sodium hydroxide or ammonium hydroxide, is added under controlled pH and temperature. This leads to the simultaneous precipitation of multiple metal ions, forming a uniform precursor. The obtained precipitate is then filtered,

washed, dried, and often calcinated to form the desired metal oxide nanoparticles. This method is simple, cost-effective, and suitable for large-scale production with good control over composition and particle size

Zinc ferrite nanoparticles were synthesized using co-precipitation method , a widely used chemical synthesize technique to prepare nanoparticles or nanocomposite , especially metal oxides like ferrites.

Initially , 5.406 g of FeCl₃·6H₂O (M=270.3 g/mol) was dissolved in 200 mL of distilled water to prepare a 0.1 M solution. Simultaneously ,1.3628 g of ZnCl₂ (M=136.28 g/mol) was dissolved in 200 mL of distilled water to make a 0.05 M solution . Both solutions were mixed under constant magnetic stirring at 80°C. . To this , 6.4 g of NaOH (M=40 g/mol) in 400 mL of water was added dropwise using a burette , forming a precipitate while maintaining the temperature around 80°C.

For silver incorporation , 0,6794 g of AgNO₃(M=169.87 g/mol) was dissolved in 400 mL of distilled water (0.01 M), and 11.764 g of (TSC)trisodium citrate (M=294.1 g/mol) was dissolved in 400 mL of distilled water to make a 0.1 M solution . Both were added to the previous mixture and stirred for 15 minutes . The final mixture was kept in hot air oven at 80°C for 2 hours , then centrifuged at 6000 rpm(rounds per minute) and dried at 100°C for 2 hours .The dried sample was ground into powder and calcined at 700°C for continuous 6 hours and sample was named as cs1 700 , similarly cs2 800 was made by similar procedure only the calcination temperature was carried out at 800°C for continuous 6 hours.

2.2. ANALYTICAL METHODS UTILIZED

2.2.1. X-RAY DIFFRACTION TECHNIQUE

X-ray Diffraction (XRD)acts as a widely employed analytical technique which serves to examine the morphological , crystallographic , and phase -dependent features of materials.It is quite important to nanomaterials research,giving some valuable insights about phase identification , crystalline size , with lattice parameters, as well as the degree of crystallinity , X-rays that are single frequency interfere in a totally constructive way, This technique is caused by several periodic crystal lattice planes that are inside any crystalline substance.A certain diffraction pattern, is being produced at the time when X-rays interact with these planes and it is property of the internal structure of the material .

X-ray diffraction (XRD) is used to study the internal structure and phase composition of various materials, particularly nanomaterials. It works on the basis of Bragg's Law, given by the equation;

$$n\lambda = 2d \sin\theta \qquad\qquad 2.2.1\ a$$

Where;

λ - represents the wavelength of the X-rays

d- is the distance between atomic layers in the crystal

θ- is the angle of diffraction

n- is an integer known as the order of diffraction.

When x-rays strike a crystalline solid, they interact with the lattice atoms and undergo scattering.If the scattered waves are in sync under specific geometric constraints, they exhibit constructive interference, resulting in distinct diffraction maxima.These peaks offer comprehension that is of great value into the material's lattice structure, even its phase purity, and also its crystallinity. X-rays can be ideal for probing distances between the atomic planes in particular. Wavelengths are within a range from 0.01 to 0.7 nanometers. An X-ray source, beam-shaping optics, a sample holder, as well as a detector that measures the intensity of scattered rays are included among the main parts of an XRD setup with a goniometer to rotate the sample. X-rays interact within the sample, diffract at different angles, the intensity results, someone records it, someone plots it against 2θ, and this reveals the sample's diffraction pattern. Diffraction peaks have a tendency to be more broad in the case of nanomaterials because crystalline domains exist in small size range.s. To estimate this size, the Debye-Scherrer equation is used :

$$\mathbf{D} = \frac{K\lambda}{\beta \, cos\theta} \qquad\qquad \textit{2.2.1 b}$$

Where,

D is the crystallite size
K is a shape factor (usually around 0.9)which is a dimensionless constant
λ is the wavelength of the X-rays
β is the peak's full width at half maximum (in radians)
and θ is the angle of diffraction (in radians)

This formula makes it possible to find correlation between the XRD peak broadening and grain size, making it especially useful when working with nanoscale materials.

2.2.2. FOURIER TRANSFORM INFRARED SPECTROSCOPY (FTIR)

Fourier Transform infrared spectroscopy (FTIR) is a widely used technique for identifying molecular groups and chemical bonds within the substances.This method provides valuable insights into molecular structure and interactions by measuring infrared radiation absorption across a range of wavelengths. The resulting spectrum serves as a unique spectroscopic fingerprint , enabling precise material characterization.

As it's core, Fourier Transform Infrared Spectroscopy (FTIR) works because molecules absorb infrared radiation at specific frequencies, triggering vibrations like stretching, bending and twisting.These unique molecular fingerprints are tied to particular functional groups, allowing for accurate identification and characterization of materials .

The technique is governed by Beer-Lambert's law.

$$A = \frac{\varepsilon}{c} \qquad\qquad \textit{2.2 a}$$

Where Absorbance relates proportionally to path length as well as concentration, while the compound's molar absorptivity is ε. The FTIR spectrum, when it is plotted versus wavenumber (cm^{-1}), as either absorbance or transmittance, acts as a fingerprint at the molecular level. We collect up the raw data as being an interferogram, then the Fourier Transform algorithm converts it into a more readable spectrum

An FTIR instrument includes several core components: an IR source (such as a Globar or Nernst glower) emitting radiation across the mid-IR region (4000–400 cm^{-1}); an interferometer that creates an interference pattern using a beam splitter and mirrors; a sample holder suited for solids (via ATR or KBr pellet), liquids (in IR-transparent cells), or gases (in long-path cells); and a detector (like DTGS for general use or MCT for higher sensitivity). The analyzed spectrum gives certain useful insights upon molecular bonding, functional groups, and molecular interactions. substance identification accuracy is improved by comparative analysis against spectral libraries.

2.2.3. UV-VISIBLE SPECTROSCOPY

UV-Visible (UV-Vis) spectroscopy is a method of analytical technique, used widely for examining the response of substances with ultraviolet and visible light. The technique generally involves radiation transmission from 190 up to 900 nm through a given sample. Part of this technique is also quantifying how much light is absorbed or transmitted. The resulting spectrum is what gives an understanding into the quantity and chemical surroundings, as well as the electronic structure of the sample.

The light energy absorption by the molecules is the basic principle of UV-Visible spectroscopy. Wavelengths, in amounts, are absorbed by a sample of molecules when UV or visible light passes through as the molecules' electrons are excited from lower to higher energy levels. The detector is in receipt of the remaining amount of light, as it does continue onward through the sample. The comparison of the intensity of incoming light with transmitted light creates an absorbance spectrum plotted as absorbance vs wavelength .

This technique follows the "Beer-Lambert Law". Absorbance is directly proportional to the concentration of the absorbing species, as well as the light's path length, plus the

substance's molar absorptivity at a specific wavelength.Accurate determination of unknown sample concentrations can be achieved by analyzing absorbance values and utilizing calibration curves or reference data.UV-Vis spectroscopy is particularly valuable for quantitative analysis in solutions, making it a reliable tool in research and industrial settings.

UV-Vis spectroscopy is also crucial in studying the optical properties of materials , especially semiconductors , using the Tauc plot.

A Tauc plot is a method used to determine the optical band gap (Eg) of a material. It is constructed by plotting $(\alpha h\nu)^n$ versus $(h\nu)$.

Where,
    α = absorption coefficient
    h = Planck's constant
    ν = frequency of the light
    n = a constant that depends on the nature of the electronic transition (e.g., n = 2 for direct allowed transitions, n = ½ for indirect allowed transitions).

From the tauc plot linear region is extrapolated to the x-axis (hv axis), and the intercept gives the band gap energy (Eg) of the material.

Inference from the Tauc plot :

·   The band gap energy (Eg) value provide critical information about the materials electronic structure
·   A smaller band gap better absorption of visible light , which is important for applications like photocatalysis , solar cells , and opto-electronic devices
·   By comparing band gaps , one can assess modifications in material properties due to doping , composting , or structural changes .

2.2.4. PHOTOLUMINESCENCE (PL)

Photoluminescence (PL) Spectroscopy is certainly a powerful, non-destructive technique used so as to investigate nanomaterials, insulators, as well as semiconductors, and especially the materials' structural and electronic properties. It provides the understandings into the band gap energy, defect states, impurity levels, as well as crystal quality. It is in the further development of such devices such as LEDs, and also laser diodes, as well as solar cells, where it is completely indispensable. PL is important to nanotechnology and optoelectronics research, helping to assess uniformity, material purity, and defect density, and uniformity, which are crucial for optoelectronics and nanotechnology research.

A normal PL configuration uses a source of excitation that illuminates the sample with light, like a laser. Photons get re-emitted at any point in time when the sample absorbs some

of this light on account of electron-hole recombination. This emitted light is collected, as well as a spectrometer analysing it, thus revealing key details regarding the material's band structure and optical properties.

One main advantage of PL is that it's non-intrusive and highly sensitive so it can detect even small defects in it. Careful control of the measurement conditions for obtaining accurate results is required, but it is mainly applicable to optically active materials.

Photoluminescence is defined by a material's excitation and emission of light. This defines a certain working principle. Each material illuminated with light having energy equal to or greater than its bandgap sees electrons in the valence band absorb this energy. These electrons then jump into the conduction band, and charged holes are left behind. These excited electrons do eventually lose some energy, recombine with all the holes, and further emit light. The energy of the emitted photons gives understanding into both its bandgap and defect states, as it reflects the electronic transitions that are within the material.

The energy of the emitted light can be described by the equation:

$$\mathbf{E = h\nu = E_g - E_{defect}} \qquad\qquad \mathbf{2.2.5\ a}$$

where Eg the band gap energy and E_{defect} accounts for any defect or impurity levels that participate in the recombination. Usually, the PL emission divides into near-band-edge (NBE) emission since excitons recombine near the bandgap, and deep-level emission **(DLE),** that originates from structural defects or impurities.

2.2.5. VIBRATIONAL SAMPLE MAGNETOMETER (VSM)

A Vibrational Sample Magnetometer (VSM) measures the magnetic properties of materials as well as is an important tool used particularly for magnetic moment, also for magnetic susceptibility. The study of several complex magnetic structures, some nanomaterials, and a few thin films, along with ferromagnetic, paramagnetic, and diamagnetic materials, applies this technique widely. With VSM, magnetic materials can be characterized at various different temperatures. Variable magnetic field strengths also render VSM especially useful for applications. It plays such a major role within material science and nanotechnology and also condensed matter physics through providing more reliable, more precise measurements of magnetization.

The principle behind a VSM relates a sample's magnetization as well as just how it responds to an external magnetic field. In a VSM setup, the sample is vibrated in the direction that is perpendicular to the field applied while being subjected to a magnetic field. The particular sample's vibration causes some magnetization. A close pick-up coil has a voltage induced into it at that point. The magnetic moment of the sample is that to which this voltage

is directly proportional. By analyzing the induced voltage signal, one can determine the sample's magnetization as a function of the applied field strength.

The VSM measures the magnetic moment of the sample by recording how the induced voltage changes, relating to the rapidity of the changes in the sample's magnetization. VSM offers sensitivity to small amounts of material as well as its operation spans across a broad range of magnetic fields and temperatures. This provides certain detailed understandings into such a sample's magnetic behavior.

2.2.5. FIELD EMISSION SCANNING ELECTRON MICROSCOPY (FE-SEM)

Field Emission Scanning Electron Microscopy is an advanced technology used to capture the microstructure image of materials. It helps to visualize very small topographic details on the surface or entire or fragmented objects. FE-SEM is normally performed in a high vacuum because gas molecules tend to disturb the electron beam and the emitted secondary and backscattered electrons used for imaging. In order to characterise the specimens in this study, Zeiss Crossbeam 340 was used to capture the microstructure image. The specimens (except powder) were cut into smaller sizes of about 5x5x5 mm and coated using aurum prior to the morphological observation.

FESEM is a microscope that works with electrons instead of light. The electrons are liberated from a field emission source and accelerate in a high electric field gradient. The object is scanned by electrons according to a zig-zag pattern. The FESEM images a sample surface by raster scanning over it with a high-energy beam of electrons. The electrons interact with the atoms comprising the sample to produce signals that contain information about surface topography, composition and other properties, such as electrical conductivity.

Its design and operation are based on principles that distinguish it from conventional scanning electron microscopes (SEMs). The experimental setup includes an electron source, electron column, simple chamber, detector, vacuum system, and control system and display. The field emission gun emits electrons under a strong electric field. Electromagnetic lenses focus the electrons into a fine beam. Scan coils deflect the beam in a raster pattern over the sample surface. As the beam interacts with the sample, various signals (secondary electrons, backscattered electrons, x-rays) are emitted and detected. The detected signals are processed to form high resolution images of the sample surface.

2.3. APPLICATIONS

2.3.1. ANTIBACTERIAL STUDIES

Antibacterial testing is crucial for assessing a material's ability to inhibit or kill bacterial growth, supporting the development of new antimicrobial agents for healthcare, food safety, and environmental protection. In our project, the well diffusion assay was utilized, which is a sensitive and effective method especially suited for nanoparticle-based compounds like Zinc ferrite/silver/silver chloride nanomaterials.

In this method, bacterial cultures of *Escherichia coli* (E. coli) and *Staphylococcus aureus* (S. aureus) were uniformly spread on Mueller-Hinton agar plates. Wells were carefully created in the agar, and test samples were introduced into these wells. Plates were then incubated at 37°C for 18–24 hours. The formation of clear inhibition zones around the wells indicated the antibacterial effectiveness of the tested materials. Compared to traditional disk diffusion, the agar well diffusion method allows for a larger volume of test material to be introduced, making it especially useful for samples with lower diffusion capabilities. Proper well formation and consistent bacterial seeding are critical for accuracy and reproducibility.

Antibacterial materials have widespread applications in healthcare, food preservation, and water treatment. For example, antimicrobial coatings on medical devices help prevent infections, antibacterial packaging extends food shelf life by reducing microbial contamination, and antibacterial agents in water treatment kill harmful pathogens to ensure safe drinking water. With the rise of antibiotic resistance, ongoing antibacterial analysis is crucial for developing effective, sustainable antimicrobial solutions.

2.3.2. OXYGEN EVOLUTION REACTION (OER)

Oxygen evolution reaction is a complex process that helps generate clean hydrogen through water splitting , a key component of many energy storage and conversion technologies. OER is naturally slow and demands a lot of energy , making it a major challenge in clean energy technologies. Relentless efforts are focused on developing smarter, more efficient catalysts that minimize energy losses and accelerate reactions for smoother, faster performance.". Innovative materials like transition metal oxides (e.g., zinc ferrite), nanostructured materials, and hybrid systems are being explored to drive advancements.. These materials show promising results due to their enhanced surface area , conductivity and active sites. To assess OER performance, techniques like Linear sweep voltammetry(LSV) and Tafel plots are used. These methods help to determine the catalyst's efficiency, kinetics and durability. The primary result is typically presented as a polarization curve obtained from Linear sweep voltammetry (LSV), where current density(mA/cm^2) is plotted against applied potential (V vs RHE). The shape of the curve gives insight into the efficiency and kinetics of the reaction. Tafel plot (overpotential vs log(current density)) is often derived from the LSV data to determine the Tafel slope, which provides information about the reaction mechanism

and the catalyst's rate-determining step. Together these plots help to evaluate and compare the performance, activity, and stability of different catalysts under OER conditions .

The setup for the Oxygen Evolution Reaction (OER) typically involves an electrochemical cell, where the reaction occurs at the anode in an aqueous electrolyte.

Electrochemical Cell:

Three-Electrode System: The most common setup is the three-electrode system, which consists of:

- Working Electrode : This is where the OER takes place. It holds the catalyst material (such as zinc ferrite/silver/silver chloride nanocomposite). And glassy carbon is used as the working electrode(3 mm diameter)coated with electrocatalyst using a Nafion binder
- Counter Electrode : A platinum electrode (Pt) is used. It acts to complete the circuit by providing a place for the counter-reaction (reduction or oxidation) to occur.
- Reference Electrode : A standard reference electrode Ag/AgCl electrode is used to measure the potential applied to the working electrode relative to a stable reference.

Electrolyte:

- An aqueous solution of 0.5 M H2SO4 is used, as it provides the necessary ionic conductivity for the OER to take place.
- For alkaline conditions, a KOH solution is used, and for acidic conditions, an H2SO4 solution is used.

Here , Linear Sweep Voltammetry (LSV) was performed at a scan rate of 5 mV/s without iR(internal resistance) corrections.

Potential values were calibrated to Reversible Hydrogen Electrode (RHE) using the nernst equation: $E(V \text{ vs RHE}) = E(V \text{ vs Ag/AgCl}) + 0.059 \times pH + 0.197$

Improving OER is vital for advancing sustainable energy technologies. As global energy demands rise, developing cleaner alternatives to fossil fuels is crucial for a greener future.

2.3.3. THERMAL DIFFUSIVITY

The photothermal effect involves the conversion of absorbed light into heat by a material through non-radiative decay. In the context of nanomaterials, this effect is particularly significant due to their strong light absorption and thermophysical properties.Zinc ferrite/silver/silver chloride ($ZnFe_2O_4/Ag/AgCl$) nanocomposites exhibit strong photothermal behavior owing to the combined effect between their components. Silver nanoparticles enhance light absorption via surface plasmon resonance , while zinc ferrite and silver chloride contribute to electron-hole separation and stability. This photothermal property can be

effectively utilized in applications such as photocatalytic reactions, energy conversion, and pollution clean up.

[4]Thermal lens spectroscopy was employed to estimate the thermal diffusivity of the synthesized sample. The nanofluids of synthesized samples were prepared in water with a concentration of 1gL-1 . The fluid contained in a sample cell was placed near the focal plane and pumped with a laser beam matching the absorbance of the sample. The variation in refractive index constitutes a thermal lens in the medium which depends on the rise time of the excitation pump pulse and also on the thermal time constant of the medium. As a consequence when the probe laser (wavelength away from the absorption edge) passes through this path, it gets expanded and the corresponding fall in intensity of the beam is monitored. The change in probe beam intensity I(t) with time t is given by 2.3.3a. The parameter θ depends on radiated thermal power (Pth), laser wavelength (λL), thermal conductivity (k), temperature dependent refractive index gradient (dn/dT) and characteristic time for thermal lens formation (tc) given by 2.3.3b. It can be calculated using 2.3.3c and 2.3.3d where I0 and I∞ are the initial and steady-state intensity of the probe signal respectively. Fitting the experimental intensity using the 2.3.3e gives the time constant (tc) as explained in an earlier report on thermal blooming. The thermal diffusivity (D) of the sample can hence be determined using after standardizing with base fluid

$$I(t) = I_0 \left[1 - \frac{\theta}{\left(1 + \frac{t_c}{2t}\right)} + \frac{\theta^2}{2\left(1 + \frac{t_c}{2t}\right)^2} \right]^{-1}$$

2.3.3a

$$\theta = \frac{P_{th}\left(\frac{dn}{dT}\right)}{\lambda_L k}.$$

2.3.3b

$$\theta = 1 - (1 + 2I)^{1/2}.$$

2.3.3c

$$I = (I_0 - I_\alpha)/I_\alpha.$$

2.3.3d

$$D = \frac{\omega^2}{4t_c}.$$

2.3.3e

[4] Pius, M., Francis, F., & Joseph, S. (2023). Enhanced thermal diffusivity and photocatalytic dye degradation capability of zinc ferrite/silver/silver chloride nanocomposites. *Journal of Nano Research*, *78*, 59-72.

CHAPTER 3

RESULTS AND DISCUSSIONS
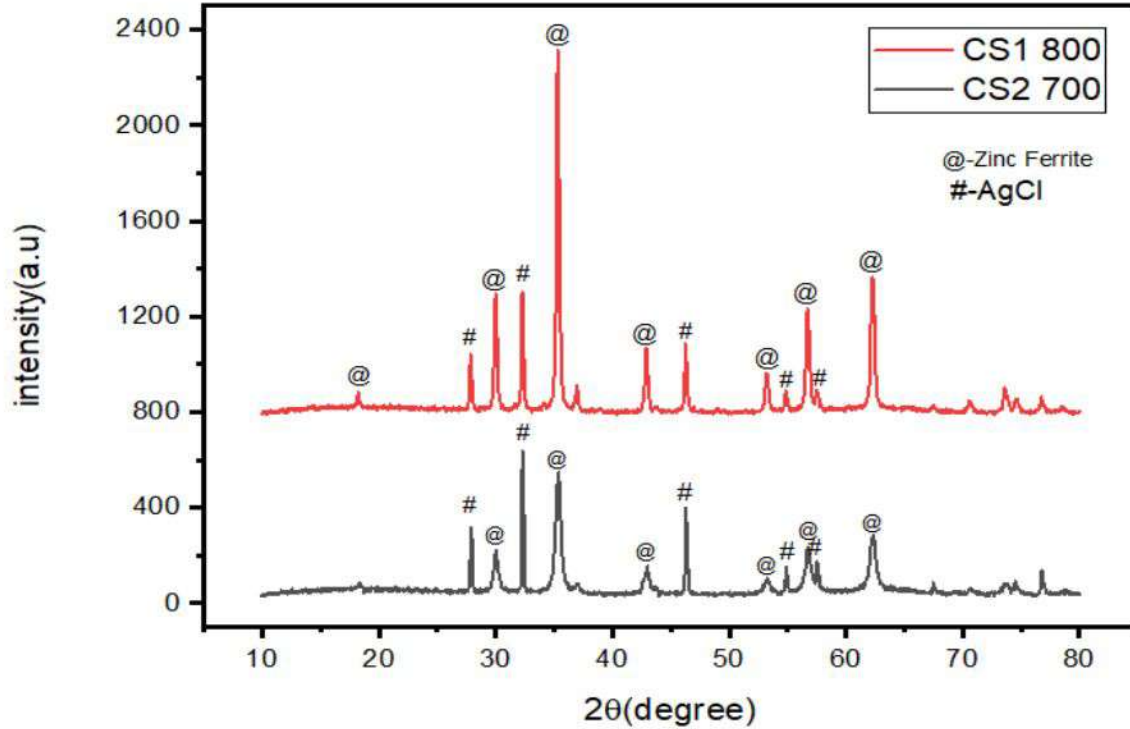
3.1. X-RAY DIFFRACTION STUDIES

Figure 4:XRD pattern of nanocomposite samples cs1 and cs2 where synthesized at 700^{0}C and 800^{0}C

The XRD patterns of nanocomposite samples calcined at 700^{0}C(cs1) and 800^{0}C(cs2) are shown in figure 4.Both the sample exhibit well defined diffraction peaks, indicating crystalline nature. The diffraction peaks observed at 2θ values of 18.3^0,30.0^0,36.3^0,42.9^0'53.2^0,56.7^0,62.3^{0}as shown in the figure 4 were indexed to the fcc lattice planes of (hkl) values (111), (220),(311),(400),(422),(511) and (440) of Zinc ferrite(ZnFe$_2$O$_4$), respectively, when compared with the JCPDS file no:00-022-1012.These peaks correspond to a face centered cubic(fcc) structure, confirming the formation of the spinel phase with Fd-3m (227) space group

A noticeable shift in the diffraction peaks toward higher 2θ angles was observed in the sample cs2 compared to cs1.This shift in peaks indicates a reduction in lattice parameters suggests improved crystallinity and densification due to thermal treatment, likely resulting from grain boundary fusion and internal stress relaxation during calcination.

In addition to zinc ferrite peaks, the sample cs2 and cs1 exhibited additional reflections corresponding to AgCl, with characteristic peaks of $27.9^0, 32.3^0, 46.3^0, 54.8^0, 57.5^0$, which match the (hkl) planes of (111) , (200) , (220), (311) , (222) respectively, and these match well well with the JCPDS No.01-071-5209, confirming the formation of AgCl with cubic symmetry belonging to the Fm-3m(225) space group.

The crystalline size(D) was calculated using Debye scherrer formula given by 3.1a ,An increase in crystalline size for Zinc ferrite in cs2 sample compared to cs1, likely due to the reduction in lattice strain.

$$D = \frac{0.9\lambda}{\beta cos\ \theta} \qquad\qquad 3.1a$$

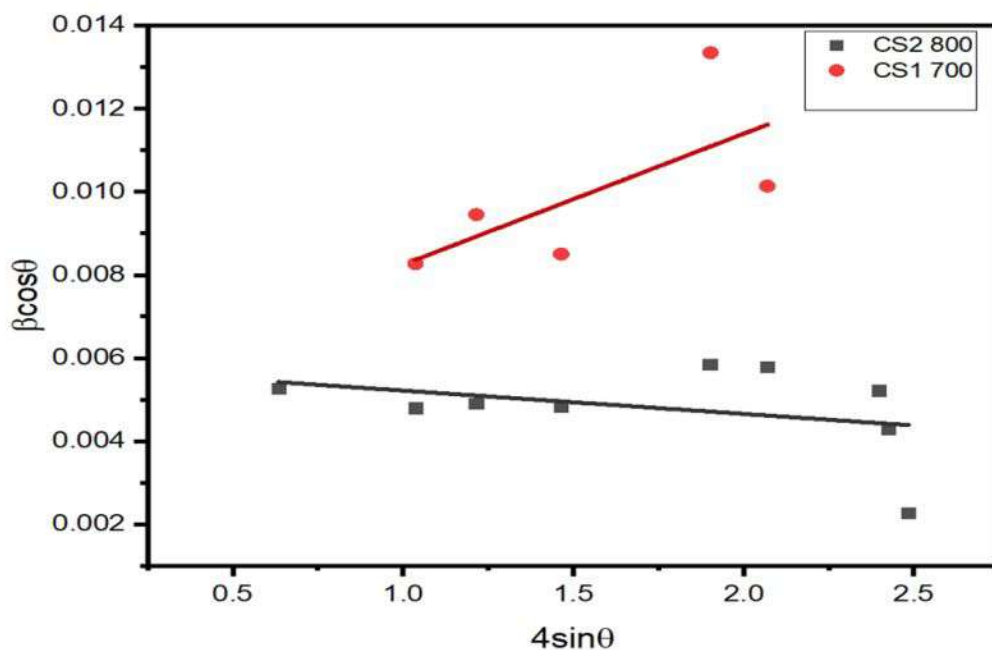| Sample	Crystalline size (Debye scherrer) (nm)			Lattice strain (W-H plot)		Crystalline size (W-H plot)
	$ZnFe_2O_4$	AgCl	Ag	$ZnFe_2O_4$	AgCl	$ZnFe_2O_4$
cs1 700	14.36 nm	44.36 nm	-	0.00315	0.0026	27.17 nm
cs2 800	28.84 nm	36.3 nm	-	0.00578	0.00545	23.98 nm

Table-1

Fig.5 : W-H plot

The crystalline size was also calculated using the cauchy's equation given by 3.1b. The slope and intercept value from Williamson-Hall plot drawn between β cosϴ on y-axis and 4 sinϴ on X-axis as in figure 5. The scherrer method yields smaller size for Zinc ferrite as it only considers peak broadening due to size and ignore strain and instrumental effects, the W-H method which accounts for both size and strain, gave more realistic values highlighting the limitations of the sherre approach.

The W-H analysis also revealed tensile strain in all samples.The increasing strain at higher calcination is likely due to grain boundary merging,enhanced defect density, dislocations, stacking faults , or sinter stress caused by prolonged thermal treatment.

At higher calcination temperature promotes crystallite growth and structural ordering , it also induces lattice strain due to thermally driven microstructural rearrangements.

$$c = \frac{k\lambda}{D}$$ 3.1b

This is the cauchy's equation used to find crystalline size from W-H plot where, D is Crystalline size calculated using Debye scherrer formula.

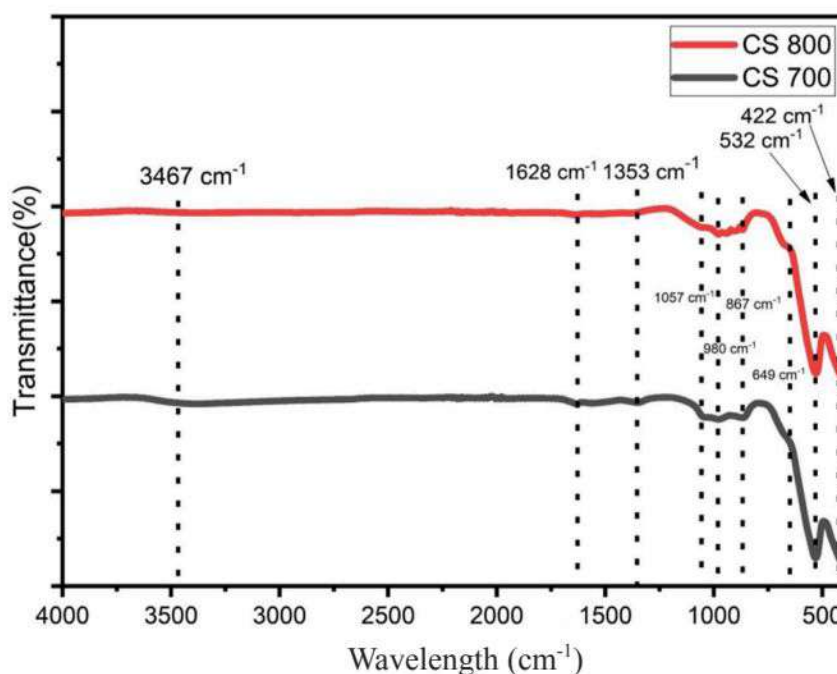## 3.2. FOURIER TRANSFORM INFRARED SPECTROSCOPY (FTIR)

Fig.6 : FTIR spectra for cs1 700 and 800

The FTIR spectra of the cs1 700 and cs1 800 samples are shown in the fig.6, recorded in the range of 4000–400 cm⁻¹ to identify the functional groups and bonding environments in

the synthesized nanocomposites. Both samples exhibit characteristic vibrational bands associated with metal-oxygen bonds and surface-adsorbed species.

Strong absorption bands appearing in the 500–700 cm^{-1} range are characteristic of the metal–oxygen vibrations in the spinel ferrite structure. The peak at 422 cm^{-1} corresponds to Zn–O stretching in the tetrahedral coordination environment.

The absorbance due to stretching and bending vibration of adsorbed water molecules assigned in the frequencies around 3400 and 1600 cm^{-1}, respectively, is decreased with increased calcination temperature. Changes in presence of water molecules is comparatively higher in cs1 700.

Prominent Shoulder peaks in cs1 800 shows the cations with different ionic states both on octahedral and tetrahedral sites and the corresponding encroachment of Zn^{2+} to the B site and subsequent migration of Fe^{3+} ions to A site.

Frequency	Functional group
422 cm^{-1}	Fe–O
532 cm^{-1}	Zn–O
649 cm^{-1}	C–H
867 cm^{-1}	C–Cl
980 cm^{-1}	C=C
1057 cm^{-1}	C–O
1353 cm^{-1}	O–H
1628 cm^{-1}	C=C
3467 cm^{-1}	O–H

Table.2

The FTIR spectrum of cs1 800 shows slightly sharper and more intense peaks compared to cs1 700, indicating improved crystallinity and phase purity. The reduced transmittance and better-resolved peaks suggest that higher thermal treatment enhances the formation of well-ordered metal-oxygen bonds and reduces residual organic or moisture content.
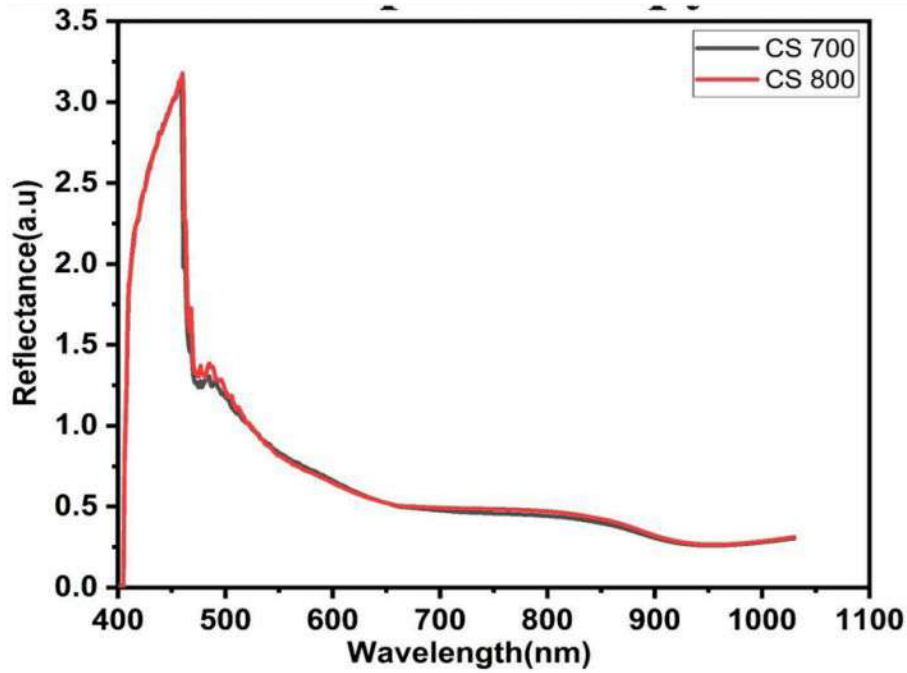
3.3. UV-VISIBLE SPECTROSCOPY

Fig.7 : absorption spectra for cs1 700 and 800

The optical properties of the cs1 700 and cs2 800 samples were studied using UV-Vis spectroscopy. The reflectance spectra for cs1 700 and cs1 800 are shown as a function of wavelength in range 400–1100 nm. Both samples show a high reflectance in the UV region around 400–450 nm, with a sharp decrease indicating intense light absorption in this range. The spectra gradually decrease with increasing wavelength, showing typical semiconductor absorption behavior. The slightly higher reflectance observed for cs2 800 compared to cs1 700 suggests a slight variation in surface morphology or particle size due to the higher calcination temperature, possibly affecting light scattering properties.
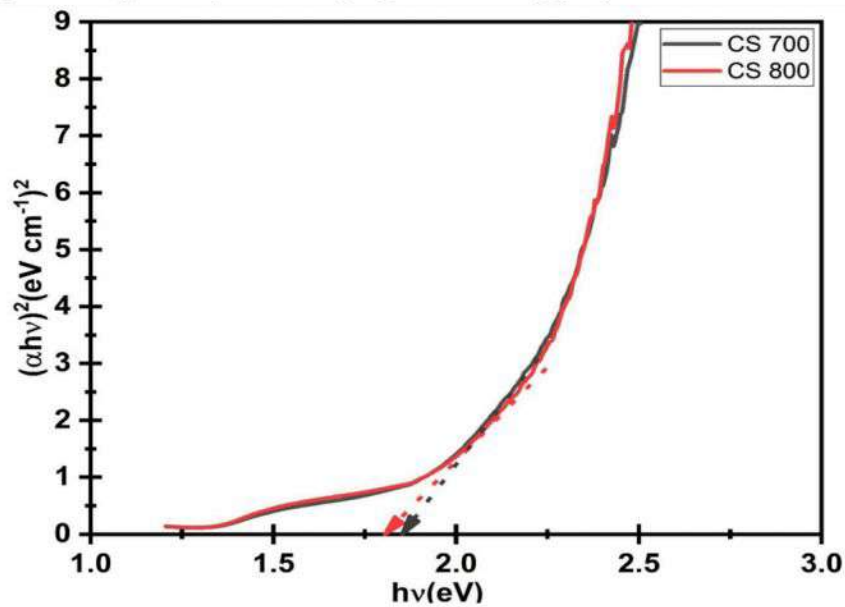

Fig.8 : Tauc plot for cs1 700 and 800

The Tauc plot, $(\alpha h v)^2$ versus photon energy $h v$, was used to determine the optical band gap of the samples, assuming a direct allowed transition. The linear region of the plot was extrapolated to the x-axis to estimate the band gap energy. The intercepts for cs1 700 and cs2 800 occur around ~2.05 eV and ~2.00 eV respectively. This slight redshift (narrowing of the band gap) in cs2 800 may result from improved crystallinity or atomic arrangement due to higher temperature treatment.

The decrease in band gap with increased calcination temperature demonstrates potential for better light absorption in the visible region, which can be useful for applications such as photocatalysis. These optical results indicate that heating the material at higher temperatures slightly changes its electronic structure, which in turn affects its interactions with light.

3.4. PHOTOLUMINESCENCE (PL)

Photoluminescence spectroscopy was used to determine the electronic structure and recombination behavior of photo-excited charge carriers in the cs1 700 and cs2 800. The photoluminescence emission of spinel ferrites is due to the charge transfer between the cation and its surrounding oxygen ions in tetrahedral and octahedral sites.

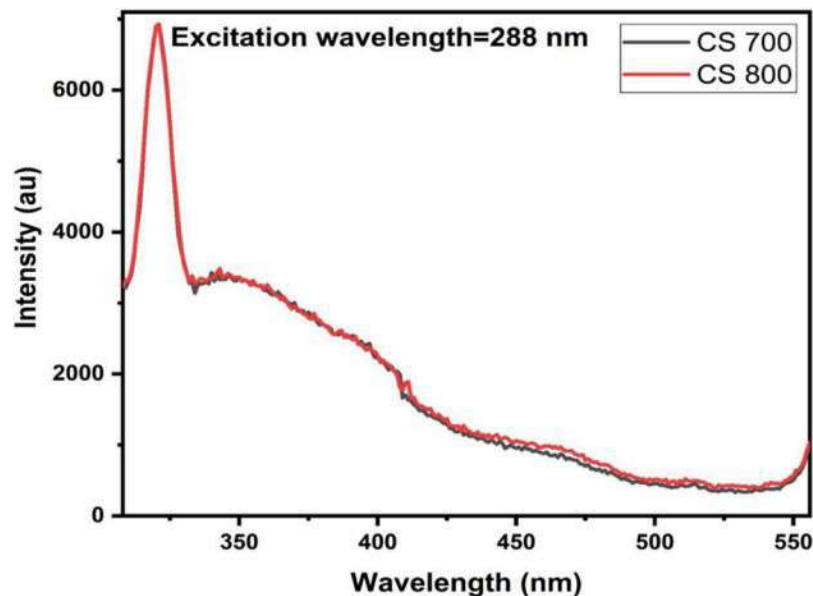The measurements were carried out using excitation wavelengths of 288 nm and 488 nm.

Fig.9 : PL emission spectra at excitation wavelength of 288 nm

The PL spectra for our samples on excitation at 288 nm shows emission peaks around 321 nm and 333 to 360 nm. Peaks around 321 nm may be due to the impurities or interstitial zinc defects. And broadband observed from 333 to 360 nm may be due to broadening of the band gap due to quantum confinement effects. The PL intensity of cs2 800 is comparatively higher than that of the cs1 700. This suggests that the higher calcination temperature may have resulted in improved crystallinity, but also potentially increased radiative recombination. The higher emission intensity could also be due to a slight reduction in non-radiative defect sites that otherwise quench the emission.
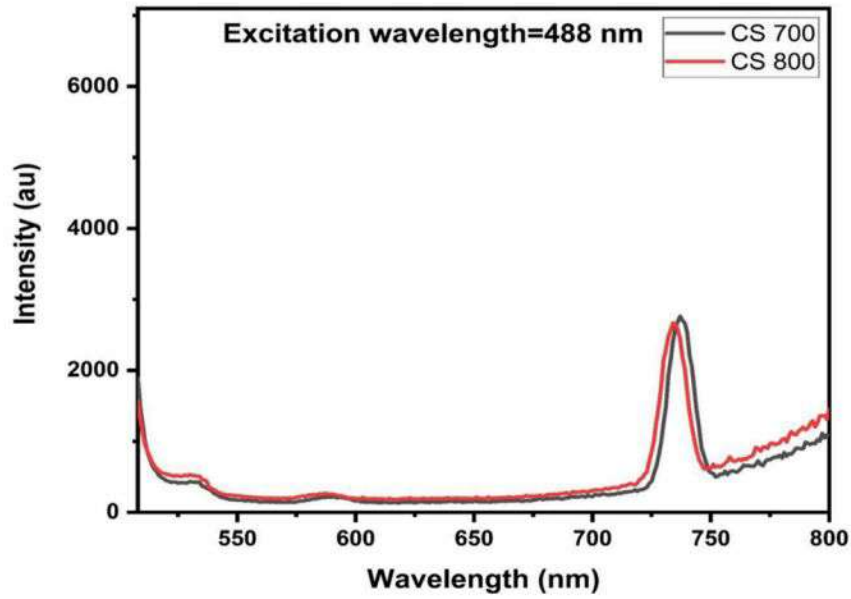
Fig.10 : PL emission spectra at excitation wavelength of 488 nm

The PL spectra for our samples on excitation at 488 nm shows emission peaks around 735 nm and 533 nm. Peaks around 735 nm may be due to stronger admixture of p-states of the neighboring oxygen atoms into the Fe^{3+} d-states. Peaks around 533 nm may be due to recombination of electrons. Here, cs2 800 exhibits a slightly lower intensity than cs1 700.

From these results we can say that increasing the calcination temperature finely tunes defect populations and carrier lifetimes, enhancing the material's potential for efficient photocatalytic and optoelectronic applications.

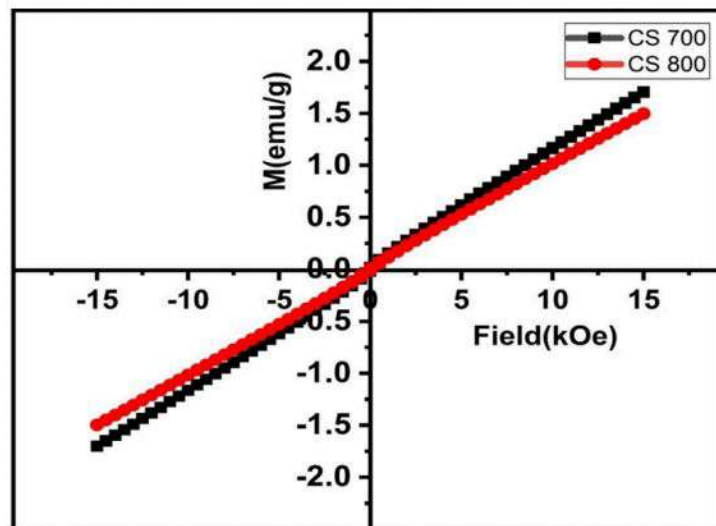## 3.5. VIBRATIONAL SAMPLE MAGNETOMETER (VSM)

Fig.11 : VSM plot for cs1 700 and 800

The magnetic behavior of the cs1 700 and cs2 800 samples was investigated using a vibrating sample magnetometer (VSM).

Sample	Coercivity (Oe)	Saturation magnetization (Ms) (emu/g)	Remanent magnetization (Mr) (emu/g)	Squareness ratio (= Mr/Ms)
cs1 700	113.82	1.71	0.2	0.12
cs2 800	82.52	1.49	0.1	0.67

Table.3

The cs1 700 sample shows slightly higher magnetization (slope of M-H curve) compared to cs2 800. That is, there is a decrease in magnetic susceptibility upon increasing the calcination temperature.

The decreased M_s value for nanocomposite samples could be due to the presence of silver chloride formed during the precipitation stage. It was found that M_s value decreased with an increase in calcination temperature, highlighting the relationship between cation migration related inversion and crystallization as well as the presence of point defects like oxygen vacancies that interfere with the A–O–B superexchange interaction between the magnetic cations in the two sub-lattice.

3.6. FIELD EMISSION SCANNING ELECTRON MICROSCOPY (FESEM)

The surface morphologies of the synthesized samples are examined using FIELD EMISSION SCANNING ELECTRON MICROSCOPY (FESEM).This technique primarily analyzes particle size distribution, surface morphology, and elemental analysis.
At 700 °C, the cs1 sample displays a homogeneous granular structure with small particles, moderate agglomeration, and a smooth surface texture, suggesting balanced grain growth and sintering.
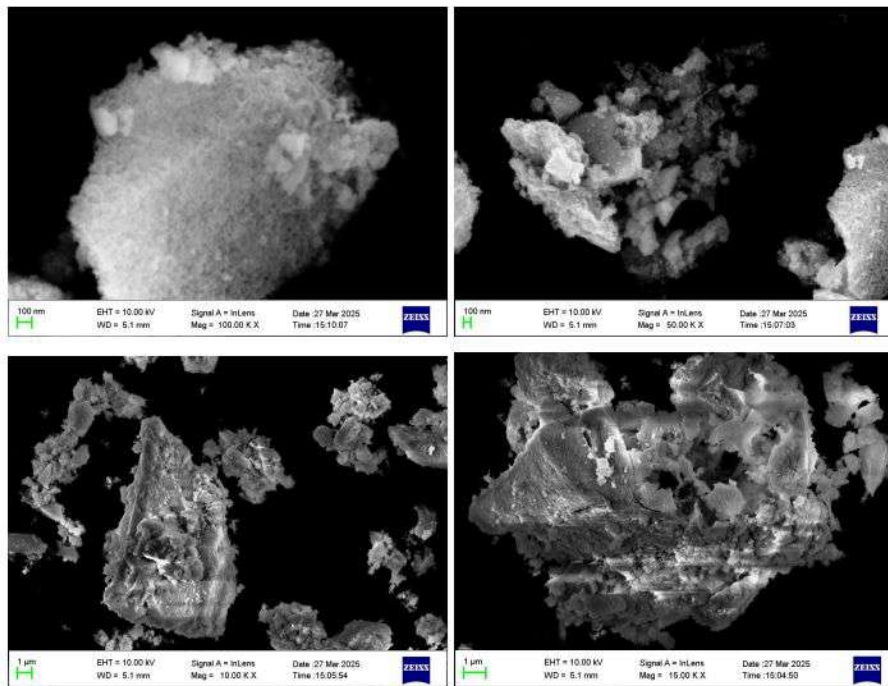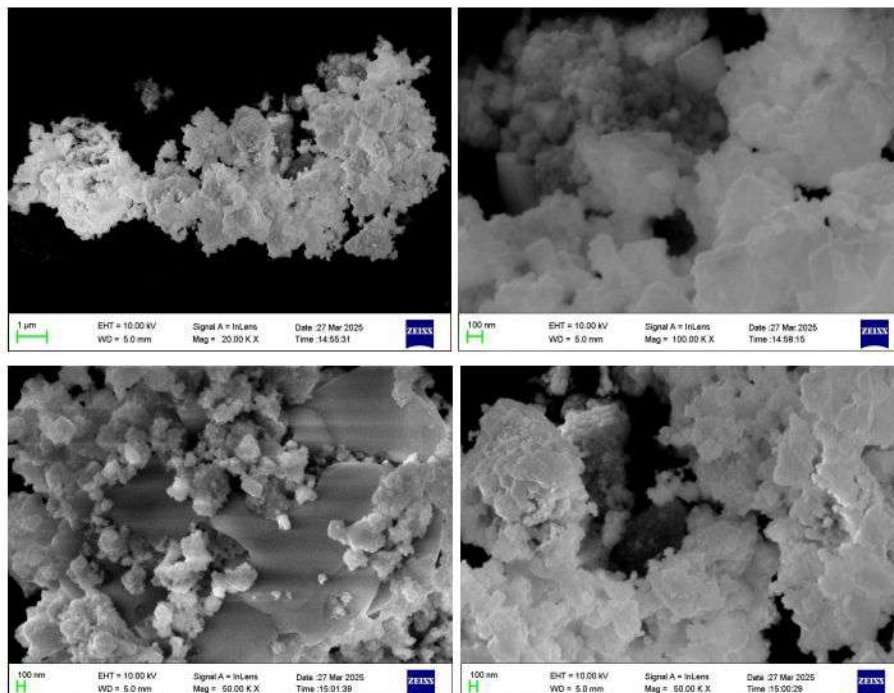
cs1 700
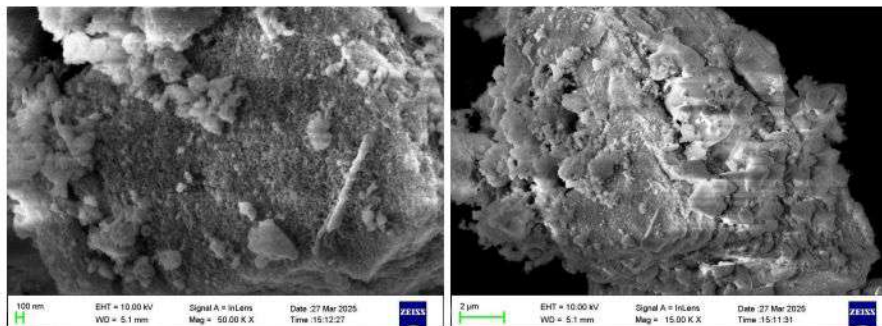
Figure 12. FESEM images cs1 700

At 800 °C, the cs2 sample shows a rough surface morphology with larger, aggregated particles and compacted grains, resulting from increased grain growth and sintering. This reduced surface area and uniformity may affect performance.
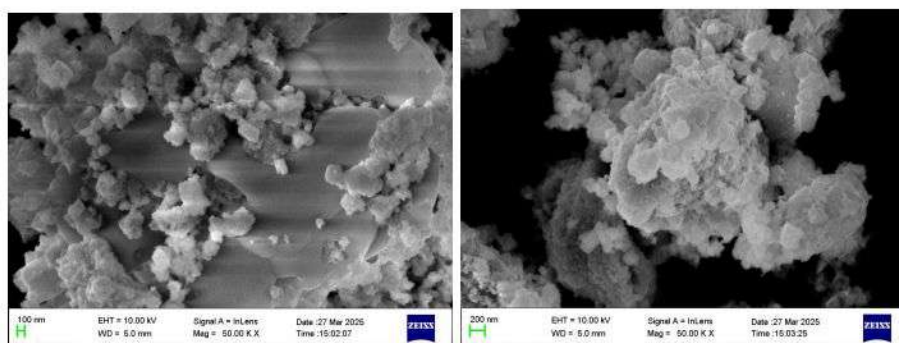
cs2 800

Figure 13. FESEM images cs2 800

3.7. ANTIBACTERIAL ACTIVITY

The antibacterial efficiency of the synthesized $ZnFe_2O_4/Ag/AgCl$ nanocomposites calcined at different calcination temperatures was evaluated using the well diffusion assay. This activity was tested against two common bacterial strains : *Staphylococcus aureus* (Gram positive) and *Escherichia coli* (Gram negative). This method is widely used to assess the efficiency of antimicrobial agents due to its simplicity, cost-effectiveness, and ability to visually demonstrate inhibition.

Four cells were created on each plate ; Well 1 which is the cs1 700 nanocomposite, Well 2 which is the cs2 800 nanocomposite, NA30 which is a standard antibiotic disc (positive control) to validate bacterial sensitivity, and DMSO which is Dimethyl sulfoxide (negative control) to ensure the solvent has no antibacterial effect.

Fig.14. Antibacterial studies

Name of the organism	Zone of Inhibition (ZOI) (cm)	
	NA30	2
	cs1 700	0.8
E.coli	cs2 800	0.8
	NA30	2
	cs1 700	1.2
S.aureus	cs2 800	1.2

Table.4

In E.coli plate;

Well 1 : shows visible inhibition zone, indicating active action against Gram-negative bacteria.

Well 2 : shows inhibition zone similar to well 2.

DMSO : shows no inhibition zone, acting as a negative control.

NA30 : shows a large inhibition zone confirming bacterial susceptibility to antibiotics.

In S.aureus plate;

Well 1 : shows inhibition zone larger than that in the E.coli.

Well 2 : shows inhibition zone similar to well 2.

DMSO : shows no inhibition zone, confirming the solvent alone doesn't contribute to bacterial inhibition.

NA30 : Shows a strong and inhibition zone, verifying the sensitivity of S.aureus to standard antibiotics.

It is important to note that the antibacterial activity of cs1 700 and 800 was evaluated using different concentrations of each sample.

The greater antibacterial effect observed against *Staphylococcus aureus* (S. aureus) compared to *Escherichia coli* (E. coli) in your experiment can be explained by fundamental differences in their cell wall structures and susceptibility to metal-based nanomaterials, particularly silver (Ag) and silver chloride (AgCl), present in your $ZnFe_2O_4/Ag/AgCl$ nanocomposites. *S. aureus* shows greater sensitivity to $ZnFe_2O_4/Ag/AgCl$ nanocomposites because;

- It lacks an outer membrane, allowing easier penetration of antimicrobial agents.
- Its thick, porous peptidoglycan layer does not block nanoparticle or ion diffusion.
- The electrostatic interaction between nanoparticles and the bacterial surface is stronger.

This makes *S. aureus* more susceptible to damage caused by $ZnFe_2O_4/Ag/AgCl$ nanocomposites, especially under oxidative stress conditions and silver ion release.

3.8. OXYGEN EVOLUTION REACTION

The electrochemical OER activity of the synthesized samples was evaluated in 0.5 M H_2SO_4 using a standard three-electrode setup and linear sweep voltammetry (LSV) at a scan rate of 5 mV/s.All potential values were converted to the reversible hydrogen electrode (RHE) scale using the Nernst equation given by 3.8a

$$E(V \text{ vs RHE})=E(V \text{ vs Ag/AgCl})+0.059\times pH+0.197 \qquad 3.8a$$
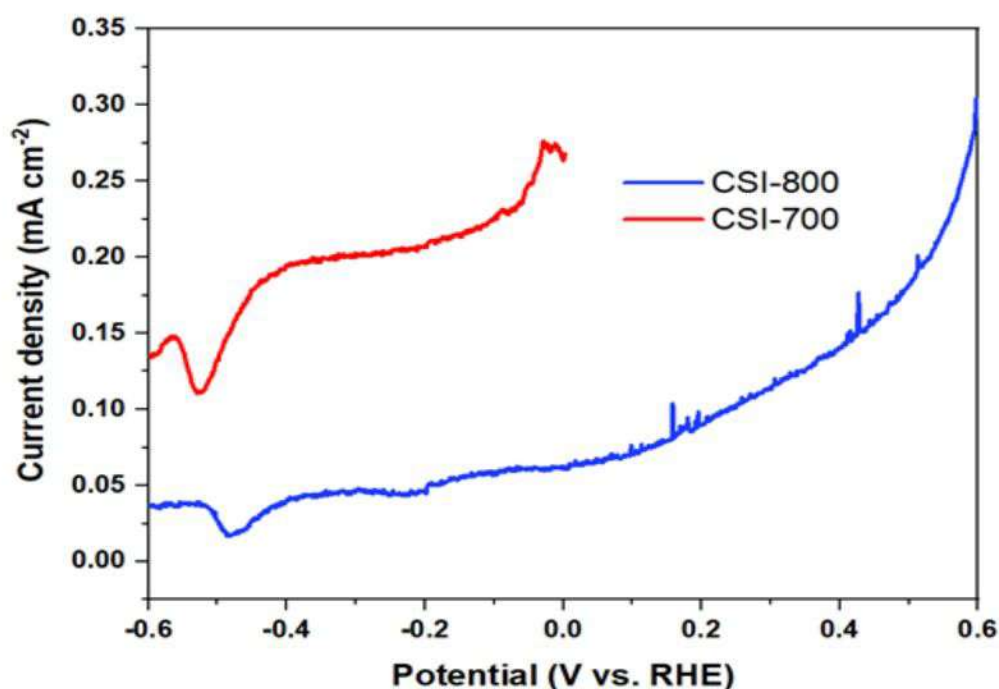
Figure 15

From the LSV plots, it is evident the cs2 800 exhibit significantly enhanced OER performance compared to their lower-temperature counterparts(cs1 700),

Cs2 shows a steep rise in current density,indicating superior catalytic activity and faster oxygen evolution kinetics.cs1 700 shows flat response with minimal current density, suggesting poor electrocatalytic performance

The higher performance in cs2 800 may be due to improved crystallinity, enhanced electronic conductivity and higher surface reactivity respectively .

3.9. THERMAL DIFFUSIVITY STUDY

To evaluate the heat transfer efficiency and potential photothermal applications of the cs1 700 and cs2 800 nanocomposite, thermal diffusivity measurements were performed using a photothermal setup

For different volume fractions (µl/ml) of the sample dispersed in a medium. The experiment was conducted for a fixed irradiation time of 20 minutes under identical conditions.

cs1 700

time	concentration	Θ	Tc	$D_2=(D_1*t_c1)/t_c2$
20 min	0	-0.128	9.3750*10^3	

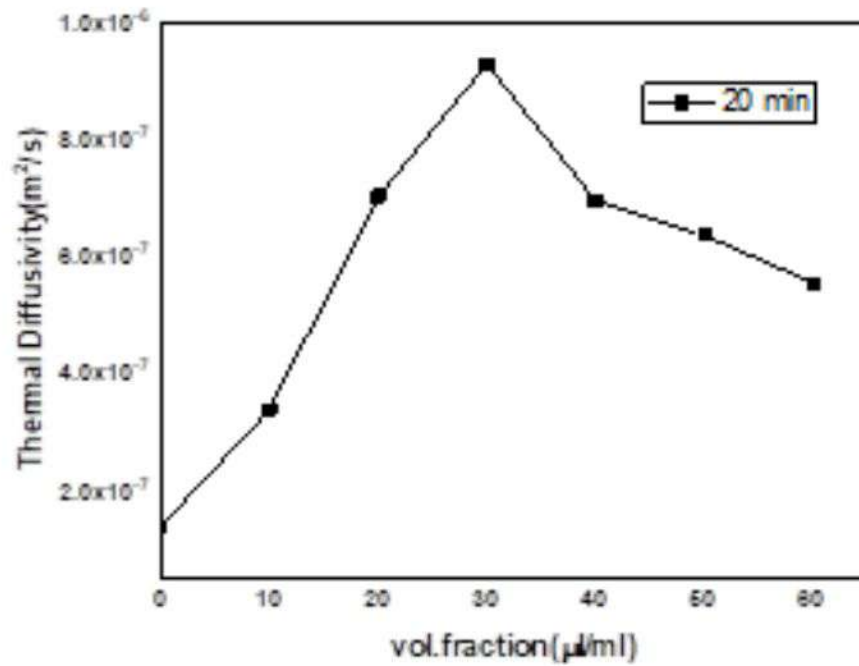|	10	-0.1124	3.8650*10^3	3.3958*10^-7
	20	-0.0972	1.8640*10^3	7.0413*10^-7
	30	-0.0858	1.4117*10^3	9.2973*10^-7
	40	-0.1028	5.2545*10^3	6.9689*10^-7
	50	-0.1457	5.7442*10^3	6.3748*10^-7
	60	-0.0566	2.3625*1063	5.5555*10^-7

Table 5

Figure 17 (plot for cs1 700)

The tabulated data and corresponding graph reveal a non-linear trend in thermal diffusivity with increasing concentration.Notably, the thermal diffusivity values increase from 1.7×10^{-7} m²/s at 0 µl/ml to a peak value of 9.3×10^{-7} m²/s at 30 µl/ml, followed by a gradual decline with further increase in volume fraction.

The 30 µl/ml concentration yields maximum thermal diffusivity due to optimal particle dispersion and interaction. Higher concentrations lead to agglomeration,

reducing heat transfer efficiency. This optimal concentration is crucial for photothermal applications, such as solar energy harvesting or therapy.

cs2 800

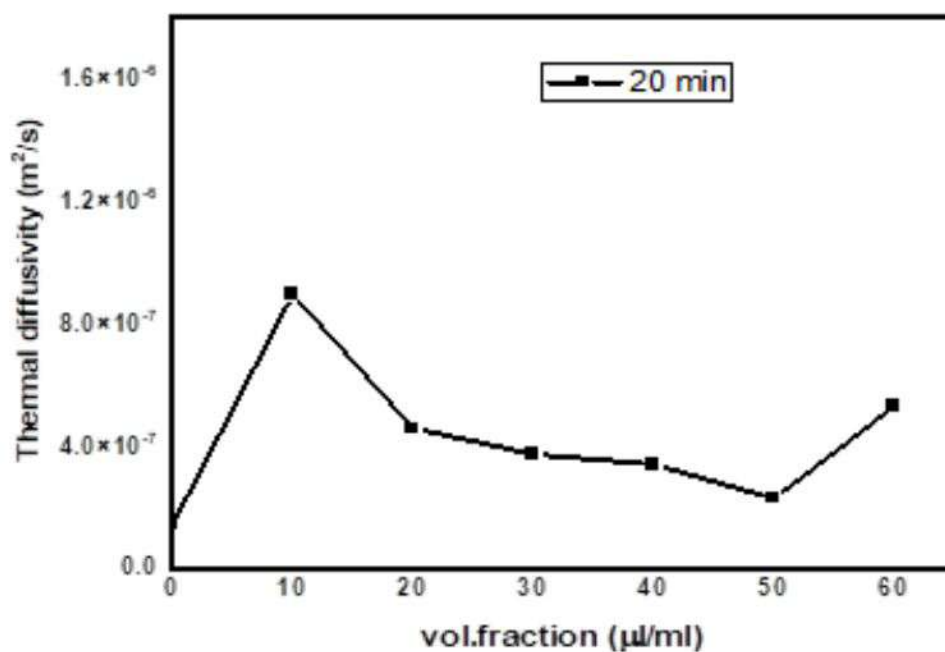| time	concentration	Θ	Tc	$D_2=(D_1 * t_c 1)/t_c 2$
20	0		3279.7	
	20	-0.2948	1005.6	4.56601E-07
	30	-0.1946	1236.9	3.71217E-07
	40	-0.1559	1356.3	3.38537E-07
	50	-0.1299	2028.9	2.26309E-07
	60	-0.0542	869.89	5.27835E-07

Table 6

Figure 17(plot for cs2 800)

The data and graph show a non-linear variation in thermal diffusivity with increasing volume fraction of the CS2 800 sample processed for 20 minutes. Thermal diffusivity rises from 1.9×10^{-7} m²/s at 0 µl/ml to a peak of 8.7×10^{-7} m²/s at 10 µl/ml, then declines to 3.1×10^{-7} m²/s at 50 µl/ml, before a slight increase at 60 µl/ml.

The peak at 10 µl/ml suggests optimal particle dispersion and interaction, enhancing heat transfer. At higher concentrations, agglomeration likely reduces efficiency by limiting surface area and contact.

This highlights the significance of optimizing nanoparticle concentration for photothermal uses such as solar energy harvesting, targeted heating in therapy, and nanofluid cooling systems.

Cs1 700 and cs2 800

Parameter	CS1-700	CS2 800
Zeta Potential (mV)	-32.1± 0.4	-32.9±0.6
Peak of Distribution (V)	-0.0287	-0.0315
Electrophoretic Mobility	-2.5009 µm*cm/V·s	-2.5349µm*cm/V s
Conductivity (mS/cm)	0.020	0.0242

Transmittance (%)	47.7	29.3841
Optical Density Filter	3.7117	3.4970

Table 7

The CS2-800 sample demonstrated superior colloidal stability compared to CS1-700, as evidenced by a more negative zeta potential (-32.9 ± 0.6 mV), increased electrophoretic mobility, and reduced transmittance. These factors collectively indicate enhanced electrostatic repulsion and improved particle dispersion. The slight rise in conductivity and marginal drop in optical density further support reduced aggregation in the CS2-800 sample. Overall, the treatment at 800 °C under CS2 conditions contributes to better physicochemical stability, which is advantageous for applications requiring stable colloidal systems.

CONCLUSION

This study successfully demonstrated the synthesis of $ZnFe_2O_4$/Ag/AgCl nanocomposites using the co-precipitation method followed by calcination at different temperatures. The materials were comprehensively characterized using techniques such as XRD, FTIR, UV-Vis, PL, VSM, and FESEM, alongside functional evaluations including antibacterial assays, photothermal analysis, and oxygen evolution reaction (OER) studies.

XRD analysis confirmed the formation of spinel phase $ZnFe_2O_4$ and cubic AgCl, with improved crystallinity at higher calcination temperatures (800°C).FTIR and UV-Vis spectroscopy revealed strong metal-oxygen bonding and a tunable band gap (~2.05 to 2.00 eV), suitable for visible light absorption.Photoluminescence analysis suggested defect-related emissions and controlled recombination behaviors influenced by calcination conditions.VSM measurements confirmed superparamagnetic nature with temperature-dependent changes in coercivity and magnetization.FESEM images highlighted morphological changes at higher temperatures, showing increased grain size and agglomeration.Antibacterial testing confirmed significant activity against both Gram-positive and Gram-negative strains, supporting the nanocomposite's biomedical potential.OER performance demonstrated enhanced catalytic activity at 800°C due to improved structural and electronic properties.Photothermal studies showed efficient heat transfer properties, indicating applicability in energy conversion and thermal therapies.Overall, the $ZnFe_2O_4$/Ag/AgCl nanocomposite exhibited multifunctional behavior, making it a promising candidate for applications in catalysis, environmental remediation, biomedical coatings, and energy devices.

FUTURE SCOPE

Scale-up and Stability Studies: Extend the synthesis to industrial-scale processes and investigate long-term stability under real operational conditions (e.g., photocatalysis in wastewater treatment).Targeted Antibacterial Applications: Explore the incorporation of these nanocomposites in medical devices, wound dressings, or packaging films for real-time antibacterial efficacy and biocompatibility testing. OER Catalyst Optimization: Further optimize the nanocomposite structure for use in water splitting devices, focusing on improving efficiency, minimizing noble metal usage, and enhancing durability in alkaline and acidic environments. Multifunctional Coatings: Study the feasibility of using these nanocomposites in coatings that simultaneously offer antimicrobial, magnetic, and self-cleaning (photothermal) properties. Mechanistic Insights: Employ advanced characterization tools such as XPS, TEM, and electrochemical impedance spectroscopy (EIS) to understand the charge transfer mechanisms and surface interactions in photocatalysis and electrocatalysis.Hybrid System Integration: Explore integration with other semiconductors (e.g., TiO_2, $g-C_3N_4$) to form hybrid heterojunctions with synergistic enhancements in optical and electronic performance.

REFERENCE

1. Pius, M., Francis, F., & Joseph, S. (2023). Enhanced thermal diffusivity and photocatalytic dye degradation capability of zinc ferrite/silver/silver chloride nanocomposites. *Journal of Nano Research*, *78*, 59-72.

2. Vinosha, P. A., Mely, L. A., Jeronsia, J. E., Monica, F. H., Raja, K., & Das, S. J. (2017). Study of Structural, optical, dielectric and magnetic properties of zinc ferrite synthesized by co-precipitation. *Nano Hybrids and Composites*, *17*, 1-9.

3. Nguyen, L. T. T., Nguyen, K. D., Nguyen, T. A., & No, K. (2022). The synthesis of zinc ferrite spinel: Determination of pH value in the co-precipitation step. *Ceramics International*, *48*(3), 4090-4095.

4. R. Raeisi Shahraki, M. Ebrahimi, S.A. Seyyed Ebrahimi, S.M. Masoudpanah, Structural characterization and magnetic properties of superparamagnetic zinc ferrite nanoparticles synthesized by the coprecipitation method, Journal of Magnetism and Magnetic Materials 324 (2012) 3762–3765.

5. J.L.M. de Vidales, A. López-Delgado, E. Vila, F.A. López, The effect of the starting solution on the physico-chemical properties of zinc ferrite synthesized at low temperature, Journal of Alloys and Compounds 287 (1999) 276–283.

6. A. Singh, A. Singh, S. Singh, P. Tandon, B.C. Yadav, R.R. Yadav, Synthesis, characterization and performance of zinc ferrite nanorods for room temperature sensing applications, Journal of Alloys and Compounds 618 (2015) 475–483.

7. A.L. Patterson, The scherrer formula for x-ray particle size determination, Phys. Rev. 56 (1939) 978–982.

8. D. Kitajima, M. Yamamoto, T. Tanabe, T. Yoshida, Real time measurements of uv-vis diffuse reflectance of silver nanoparticles on gallium oxide photocatalyst, Catalysis Today 375 (2021) 501–505.

9. N. Kislov, S.S. Srinivasan, Yu. Emirov, E.K. Stefanakos, Optical absorption red and blue shifts in znfe2o4 nanoparticles, Materials Science and Engineering: B 153 (2008) 70–77.

10. Pius, M., Joseph, N., & James, K. (2019). Enhanced antibacterial activity of novel magnetic ZnFe2O4/AgCl nanocomposites. *Materials Today: Proceedings, 9*, 70-76.

11. FATHIMA, N. V. (2022). *TEMPERATURE CONTROLLED SYNTHESIS OF ZINC FERRITES AND ITS NANOCOMPOSITES FOR PHOTOCATALYTIC AND ANTIBACTERIAL APPLICATIONS* (Doctoral dissertation, St. Teresa's College (Autonomous), Ernakulam).

12. Pius, M., Francis, F., & Joseph, S. A. (2024). Magneto-thermo-optic characterization of ZnFe2O4/Ag/AgCl nanocomposite/water nanofluid. *Journal of Materials Science: Materials in Electronics, 35*(24), 1658.